CHAPTER 8

Coupling Atmospheric and Fire Models

MARY ANN JENKINS
Department of Earth and Atmospheric Science, York University, Toronto, Ontario, Canada

TERRY CLARK AND JANICE COEN
National Center for Atmospheric Research, Mesoscale and Microscale Meteorology, Boulder, Colorado

I. Introduction
II. Vorticity Dynamics in a Fire
III. Coupling between Atmosphere and Fire
IV. The Elements of Fire Modeling
V. Modeling the Atmosphere
VI. The Coupled Fire–Atmosphere Modeling Approach
  A. The Importance of Ignition Tracing on Fire–Atmosphere Coupling
VII. Idealized Studies of Wildfire Behavior
  A. Fire-Scale Convection Drawing the Fire Line
  B. Fire-Scale Vortices Disrupt the Fire Line
  C. Microscale Vortices Affecting Fire Spread
  D. The Effect of Atmospheric Stability and Wind Changing with Height on a Fire Propagating over a Small Hill
  E. Sensitivity of Fire Behavior to Fuel Characteristics and Configuration
VIII. Infrared Observations of Fires
IX. Conclusions and Future Work
Appendix I. Circulation and Vorticity
Appendix II. Development of Vertical Rotation in a Frictionless Fluid
Appendix III. Generation of Vertical Motion in Rotating Convective Cells
Notation
References

Forest Fires

I. INTRODUCTION

The interactions of forest fires and air flow are highly nonlinear. The heat and moisture supplied through the burning of ground and canopy fuel during a forest fire create extreme levels of buoyancy forcing. The horizontal gradients of buoyancy produce vortices or fire whirls of tornado strength, which in turn affect the nature of the fire spread through advection of hot gases and burning material, while fire vortices enhance mixing of air with the flame which leads to higher flame temperatures, increased combustion efficiency, and greater intensity. Winds at the fire scale can be either strongly modified or even solely produced by the fire, depending on the level of atmosphere–fire coupling. This coupling or feedback occurs over spatial scales from tens of meters at the flame front to kilometers on the scale of the total burn area.

In this chapter, we attempt to describe a fairly recent and major advance in the modeling of wildfires: the coupling of a cloud-resolving numerical prediction model with a simple fire-spread and wildfire behavior model, so that the atmosphere–fire is treated as a single, dynamical system. With this modeling approach, it is possible to simulate the small-scale atmosphere–fire interactions and feedbacks that are important to wildfire behavior, especially severe wildfire behavior, and the possible impacts of evolving, larger scale atmospheric forcing on the fire and vice versa.

A "small" fire is more or less a surface fire, in steady state, that grows in size but not in intensity. Small fires spread through more or less constant heat transfer by radiation with additional heat transfer by convection, or winds, at the head of the fire. Small fires are governed by the properties of the fuel bed in which the fires burn and the air movements within and a few meters above the fuel bed. A small fire becomes a "large" fire when the fire's intensity becomes sufficiently great to produce a convection column stronger than the ambient wind field. A fire that multiplies its rate of energy output many times in a short period and burns with an intensity far out of proportion to apparent burning conditions is called a "blowup" fire.

Large fires do not conform to fire behavior expected of the far more frequent, low-intensity surface fire. Large fires are said to "make their own weather" because they can noticeably alter the temperature, humidity, and wind fields in their vicinity. A large fire exhibiting extreme behavior can put up a convection column to a height of 7000 m or more. Large fires and blowup fires have higher fire-line intensities (defined as a heat flux or the rate of fire line spread times the heat per unit area generated by the available fuel), where high fire-line intensities are of two forms: a high rate of spread when the fire is wind driven or high rate of heat release when the fire is convection dominated. Large fires have different modes of propagation and distribution patterns than the ordinary surface fire. Their fire fronts can have significantly higher spread rates (up

to 61 m/min as opposed to 6 m/min for surface fires with steady state headfire spread rates; McRae *et al.*, 1989) and can accelerate under the influences of convection. Convective processes in the column can produce extreme fire behavior such as crown fires or large-scale spotting caused by firebrands lofted ahead of the fire by wind. In the aftermath, the burn pattern may show complex boundaries and inexplicably unburned islands. It is the task of fire researchers to explain such behavior and patterns, and ultimately to predict them.

In some cases, a large fire becomes a conflagration, a fire that takes on storm characteristics with associated strong, mesocyclonic rotation. Massive fire whirls up to 400 m wide and several thousand meters in height can develop on the outer perimeter. Whirls on the edge of the burn can be powerful enough to rip out standing trees and send them up into the convection column. They can travel for considerable distances (4 km), removing slash pieces and organic material in their path, exposing the bare mineral soil underneath (McRae and Stocks, 1987; McRae and Flannigan, 1990). Large pieces of slash (4 m long, 20 cm in diameter) can be driven into the ground (45 cm into a sandy soil), much like spears. There is postfire evidence of multiple whirls within these burns.

Although relatively rare, blowup fires, large fires, and conflagrations are responsible for the major loss of life in forest fires (Chandler *et al.*, 1983), and in the western United States, 1% of the largest fires account for 80–96% of the area burned (Strauss *et al.*, 1989). Large-scale forest fires result in billions of dollars in financial losses annually in the United States alone. They can locally disrupt complete ecosystems and can, in cases of extremely large fires, eject significant amounts of smoke high into the atmosphere with possible long-range air quality and long-term global meteorological effects.

Each blowup fire or conflagration raises the question of how to recognize the conditions causing extreme fire behavior and how to predict them. The transition from a small fire to a large fire is typically sudden, 15 minutes or so, and at present, the causes for the sudden transition from an ordinary, steady state to large or blowup fire are not known. Wildfire behavior models developed by the forestry community have traditionally been used to predict fire spread rate and heat release for a prescribed set of fuel, slope, and wind conditions and are designed primarily to assess the behavior and risk of surface fires. These models are not capable of assessing the complex behavior and risk of fires that have progressed past the small stage.

In the following sections, the basics of coupled fire–atmosphere numerical prediction, an approach that is capable of simulating the complex behavior of large and small fires, are presented. The vorticity dynamics that play an important role in determining fire behavior are described. To define what is meant by fire–atmosphere coupling, a nondimensional Froude number, the ratio between the kinetic energy of the flow in a fire and the potential energy provided by the fire, is presented and its importance to fire dynamics and extreme fire

behavior is discussed. The elements of a fire model and of a three-dimensional numerical atmospheric prediction model, and how these models are coupled to produce a physically based dynamical fire–atmosphere model appropriate for wildfire modeling, are described. The sources of error in a numerical approach to coupled fire–atmosphere prediction, the problems of resolution, and the technical and physical difficulties to overcome are discussed. Recent numerical modeling studies of wildfire behavior using a coupled atmosphere–fire model are presented, and how infrared video technology is used to observe and analyze important physical features and properties of fire-scale convection from a safe distance is described. Finally, we discuss where the coupled fire–atmosphere modeling approach is, where it is likely to go in the near future, and what it should become.

II. VORTICITY DYNAMICS IN A FIRE

When the fire's intensity becomes great enough so that the flow responds strongly to the heating supplied by the fire, the fire can force its own fire-scale circulations. Convective eddies are seen as horizontal rolls or vertical vortices. In a convectively dominated fire, intense vertical rotors can develop, with wind speeds up to 100 m s^{-1} (Corlett, 1974; King, 1964). To understand the convective processes that come into play, we must understand the dynamics of the fluid and how these rotating rolls or vortices develop.

Vertical shear in the wind (wind speed changing with height) provides a source of rotation about a horizontal axis. To understand why, look at the situation depicted in Figure 1. Imagine a paddle wheel placed in the wind field, with the wind coming from the left. Since the wind hitting the bottom of the paddle wheel is stronger than the wind hitting the top, the wheel spins in a counterclockwise direction (Figure 1a). Similarly, parcels of air in the shear wind field rotate because the bottoms of the parcels are moving faster than the tops. This spin of individual air parcels or particles is called vorticity. When the winds begin to interact with a strong updraft, as shown in Figure 1b, the rotation about the horizontal axis is tilted, becoming rotation about a vertical axis. Similarly, the rotation of individual air parcels in the fluid is also tilted into the vertical producing vertical vorticity.

Strong horizontal gradients in buoyancy near the surface along the leading edge of the fire front produce especially strong horizontal rotation or vorticity. When the horizontal vorticity is tilted into the vertical by the fire updraft, very intense vertical vorticity can develop where the large buoyancy gradients and horizontal gradients of the vertical wind coexist.

Vertical vorticity is also produced by the solenoidal effect. In the absence of other forces, fluid parcels or particles will not spin when density and pressure fields are constant or when they change but in the same direction. But when

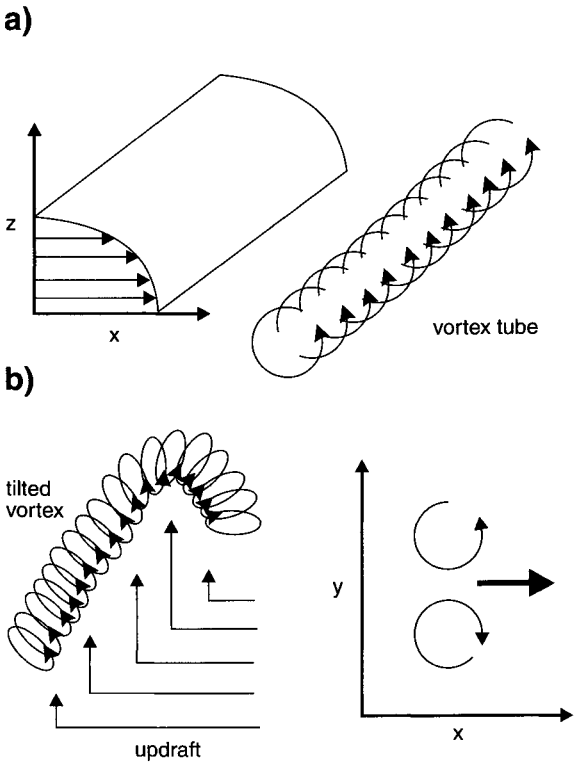

FIGURE 1 Spin about a horizontal axis, illustrated by the vortex tube, is present when wind speeds change (in this case decrease) with height (a). When the vertically sheared winds are deflected by a strong updraft (b), the axis of spin is tilted into the vertical. For the conditions depicted in (a) and (b), the resulting upflow has a counterclockwise spin to the north of the updraft core and a clockwise spin to the south.

horizontal gradients of pressure and density occur and are not parallel, fluid parcels experience opposing forces over their lengths, that combine to exert a torque, causing them to rotate, producing vertical vorticity.

To illustrate this, consider what happens to a small rectangular parcel or bar of fluid in the situation depicted in Figure 2. First imagine a pressure gradient in the fluid, perpendicular to the parcel and uniform along its length. In this case, the parcel simply moves through the fluid from high to low pressure without rotating. Now imagine that the fluid density is not constant but is larger at one end of the parcel than the other. The forces $\vec{F}_{y_1}$ and $\vec{F}_{y_2}$ acting on either end of the parcel are approximated by

$$\vec{F}_{y_1} = -\frac{1}{\rho_1}\frac{\Delta p}{\Delta y}, \qquad \vec{F}_{y_2} = -\frac{1}{\rho_2}\frac{\Delta p}{\Delta y}$$

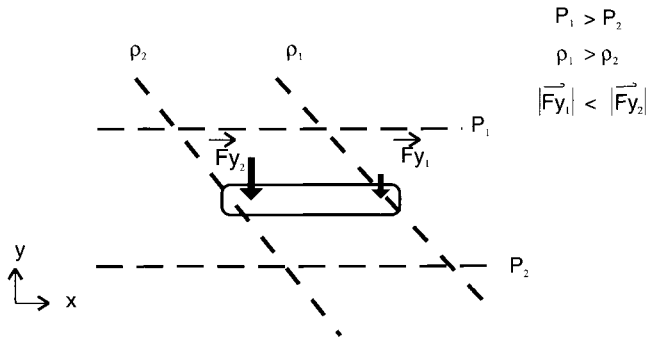

FIGURE 2 Production of vertical vorticity by the solenoidal effect. See text for explanation.

Since

$$\rho_1 > \rho_2, \qquad \frac{1}{\rho_1} < \frac{1}{\rho_2}$$

then

$$|\vec{F}_{y_1}| < |\vec{F}_{y_2}|$$

The torque applied by the forces, $\vec{F}_{y_1}$ and $\vec{F}_{y_2}$, causes the fluid bar to rotate counterclockwise. Here ρ is fluid density, and Δp is the difference in fluid pressure over distance Δy, where y is the horizontal north–south direction.

Once tilted into the vertical or generated by the solenoidal effect, vertical vorticity can be intensified by the processes of horizontal convergence and vertical stretching. Imagine an air parcel enclosed by a surface. When additional air flows horizontally through this surface into the parcel, we say that mass converges into the parcel or that the parcel experiences horizontal mass convergence. More air enters the air parcel ($u + \Delta u$ or $v + \Delta v$, where u and v are wind components in the horizontal east–west or x and north–south or y directions, respectively, and Δu, Δv, are changes in u, v) than leaves it (u or v). If no adjustment in its physical parameters follows, the parcel experiences compression or, what is the same thing, an internal pressure increase. The parcel expands to relieve this outward-directed pressure force. But the horizontal mass influx prevents horizontal expansion to a great degree, so the parcel expands or stretches vertically.

Vertical stretching and horizontal convergence also occur in the following way. Imagine a vertically spinning air parcel as a short, wide vortex tube. The vortex tube will stretch vertically if the top rises faster than the base. The difference in rise is $\Delta w/\Delta z$, where Δz is distance in the vertical and Δw is the change in vertical velocity w over Δz. When $\Delta w/\Delta z$ is positive, there is more

air leaving the top of the air parcel ($w + \Delta w$) than entering the bottom (w). This is called divergence, and the tube is being stretched vertically. But the parcel's mass must be conserved. Conservation of mass therefore requires horizontal convergence, which shrinks the tube's radius, narrowing the diameter of the spinning air parcel.

A fundamental law of physics requires that an air parcel's angular momentum about its vertical axis, which is proportional to its momentum (mass times velocity) and to its distance from the axis, be conserved. As the air parcel's distance from the central axis of rotation decreases, its velocity must increase. This is the principle of conservation of angular momentum and can be thought of as the "ice skater effect." The air parcel begins to spin faster, just as a figure skater spins faster when she pulls her arms into her body.

Horizontal convergence and vertical stretching narrow the diameter of the spinning air parcel, further increasing its rotation as the angular momentum of the air parcel, now rotating over a smaller distance, is conserved (i.e., the ice skater effect). Vertical vorticity therefore is intensified.

Vorticity can also increase or decrease at any given locality just by air with different vorticity blowing into its region. Local vorticity increases when replaced by air of greater vorticity and decreases when replaced by air of lesser vorticity. This process is called advection, and it works in both horizontal directions and in the vertical direction. The term advection is normally reserved for horizontal transport, whereas vertical advection is known as convection.

Finally, turbulent or frictional drag in a fluid can affect vorticity. Turbulent or frictional drag can sometimes increase rotation and, very importantly, sometimes reduce or even eliminate rotation in a fluid. Friction slows wind near any solid boundary such as the ground, and in this case friction always acts in the opposite direction from the wind. Frictional drag against the ground reduces rotation or causes spin-down regardless of wind direction.

A vortex is air moving around a central axis about as fast as it moves toward and along the axis. The development and intensification of a vertical vortex is a combination of multiple processes working together: the generation of vertical vorticity by the solenoidal effect and tilting, the dynamic-pipe effect, advection of vorticity in the vertical, and convergence and vertical stretching (Appendices II and III).

Figure 1 illustrates the generation of vertical vorticity by tilting. Once the horizontal vorticity in Figure 1a is tilted into the vertical (Figure 1b), the local vorticity owing to this tilting will be positive to the north of the updraft core and negative to the south. As a result, a counterrotating vortex pair is established with counterclockwise rotation to the north and clockwise rotation to the south of the initial updraft.

Along the rotating column of each vortex, the pressure field is in balance with the strongly curved wind field. The inwardly directed force acting on air

parcels as a result of the reduced pressure at the center of the column is countered by the outwardly directed centrifugal force resulting from the parcels' rotation about the center. In this condition, called cyclostrophic balance, air moves easily around and along the axis of the vortex, but radical motions toward or away from the axis of rotation are strongly suppressed. The rotating column acts as a "dynamic pipe"; it is like a hose of a vacuum cleaner, except that instead of being channeled by the wall of the hose, the airflow in the vortex is constrained by its own swirling motion.

The low pressure in the center of the vortex provides a vertically directed pressure gradient force (the centrifugal pump effect described in Appendix III). Since air is accelerated from high to low pressure, an updraft develops from below, or a downdraft develops from above, in the rotating core. When the vertical pressure gradient force directs air parcels upward, the air flowing along the vortex's axis is sucked in through its lower end, and as air parcels converge into the base of the pipe, they turn and accelerate upward. In doing so, they are stretched vertically (as in Figure 3). Stretching narrows the diameter of the vortex, further increasing the angular speed of its winds and the vorticity of its air

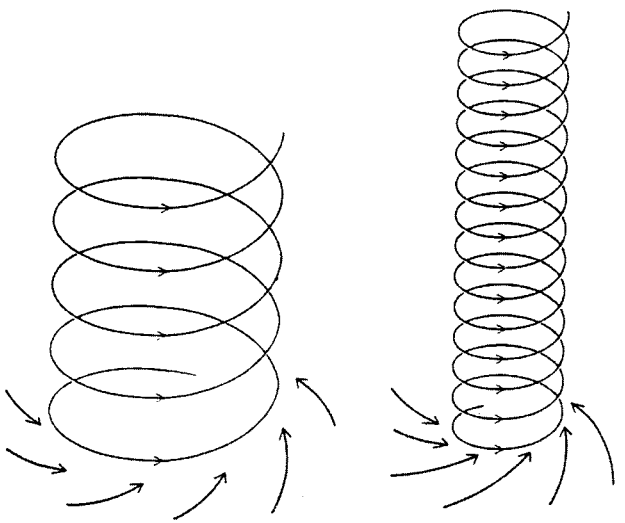

FIGURE 3 Convergence and stretching intensify the vertical rotation initiated by tilting and extend it upward. Once rotation is vertical, a balance between the inwardly directed pressure gradient force and the outwardly directed centrifugal force develops. The centrifugal force suppresses flow toward or away from the axis of rotation (the "dynamic pipe" effect), while the low pressure at the center of rotation provides a vertically directed force. When the force is directed upward, the winds converge at the lower end of the rotating updraft. The enhanced convergence compresses the column and stretches it upward. Because the column is narrower, it must spin faster to conserve its angular momentum.

parcels, as the angular momentum of the air, now rotating over a smaller distance, is conserved (i.e., the ice skater effect).

Thus, for an upwardly directed pressure gradient force, the dynamic pipe intensifies the rotation at its lower end, which in turn extends the pipe downward as the centrifugal force gets strong enough to establish cyclostrophic balance. Owing to inertia, inflow that gets sucked in through the pipe's lower end can actually overshoot its equilibrium radius, conserving its angular momentum and picking up speed as it approaches the center of the core before turning sharply to spiral upward. As a result, the vortex is narrower at the bottom, and the highest wind speeds are found in a small ring at the base of the vortex.

Frictional drag against the ground upsets the cyclostrophic balance of the vortex by slowing the wind and reducing the centrifugal force to zero. But the inward radial pressure-gradient force does not vanish there. As a result, strong inflow close to the ground, driven by the unbalanced inward pressure gradient force, transports fluid parcels closer to the axis than would have otherwise been possible without friction, whereupon the flow turns vertical. The resulting wind speeds can be significantly greater than those of the circulation in the vortex above the surface friction layer.

Note that while vertical progression due to the dynamic pipe effect can take place, the vortex can also build upward or downward through vertical advection of vorticity and intensify by convergence and stretching. When vorticity and radial inflow are constant with height, high angular momentum air approaches the axis from below and aloft simultaneously. The vortex in this case forms nearly independently of height. In a fire, however, buoyancy forcing supplied through the burning of surface fuel and the generation of near-surface vertical vorticity by the solenoidal effect and tilting likely provide that the vertical vorticity and radial inflow are maximized near the ground. Apparently due to vertical advection of vorticity and horizontal convergence and vertical stretching, the fire vortex forms from the ground upward. It is also observed that fire vortices can be short-lived. One possible explanation for this is that the pressure gradient forcing can boost updraft strength at one level, quickly destroy it at another. A detailed examination of where and what processes dominate to build and destroy fire vortices has yet to be done.

It is also possible that, as a result of powerful updrafts in the cores of vortices, compensating downdrafts form between the updraft cells, which, if strong enough, can separate and move the centers of convection to the right and left of the original updraft depicted in Figure 1b.

The vortex dynamics just presented are purposely idealized or simplified to convey the essence of the problem. A seemingly simple complication arising in reality is that rotating vortices are observed to sometimes break apart, as discussed in the next paragraph. Exactly how vortices restructure themselves in such cases is unknown and something that fire modeling may eventually resolve. Neither is the observed flow field necessarily a one-cell vortex charac-

terized by an updraft at the core of the vortex. Powerful vortices can also develop an internal multiple vortex structure that has a downdraft in the central core surrounded by two or more subsidiary vortices with updrafts along their vertical axes. To learn more about the complications of the internal structure of laboratory vortices, we refer the interested reader to Church and Snow (1979) and Gall (1982).

Vertical rotation within fires can result from at least two similar but different mechanisms. Adopting the terminology from Clark *et al.* (1999), the first mechanism is enhanced vortex tilting. In this case, the tilting of horizontal vorticity is believed to result from a local region of buoyancy that acts strongly enough to break or disconnect the tilted vortex, leaving one or two rotating, standing hot fire whirls or plumes, which transport heat almost vertically into the atmosphere.

The second mechanism is the "turbulent burst"- or "horseshoe"- or "hairpin"-shaped vortex. The turbulent burst is a concept developed in the study of boundary layer turbulence (e.g., Moin and Kim, 1982; Kim and Moin, 1986). The boundary layer is defined as the portion of the atmosphere in which the flow field is strongly influenced by interaction with the surface of the Earth. Again vortex tilting occurs, but in a manner that results in an unbroken vortex that moves both vertically and horizontally; as the vortices rise and come closer together, their combined motion results in the vortex tilting forward at a relatively sharp angle giving a hairpin shape. When the horizontal motion is strong enough, the rotors shoot or burst forward over unburned fuel, sometimes for considerable distances. It is believed that this type of vortex tilting led to the hairpin vortex observed by Radke *et al.* (2000). Observations captured a flame shooting horizontally as far as 100 m in only 2 s (Figure 4), and the fire fighters wisely stayed clear of this particular fire behavior at the time of the observations.

For a more in-depth description, a mathematical treatment of vorticity is given in Appendix I, the development of vertically rotating convective cells is described in Appendix II, and the development of an updraft in a rotating convective cell is described in Appendix III.

III. COUPLING BETWEEN ATMOSPHERE AND FIRE

As discussed in previous sections, winds at the fire scale can be either strongly modified or even solely produced by the fire, depending on the level of atmosphere–fire coupling. This coupling or feedback occurs over spatial scales from tens of meters at the flame front to kilometers on the scale of the total burn area. Therefore, the knowledge of the interaction of the fire with the atmosphere is

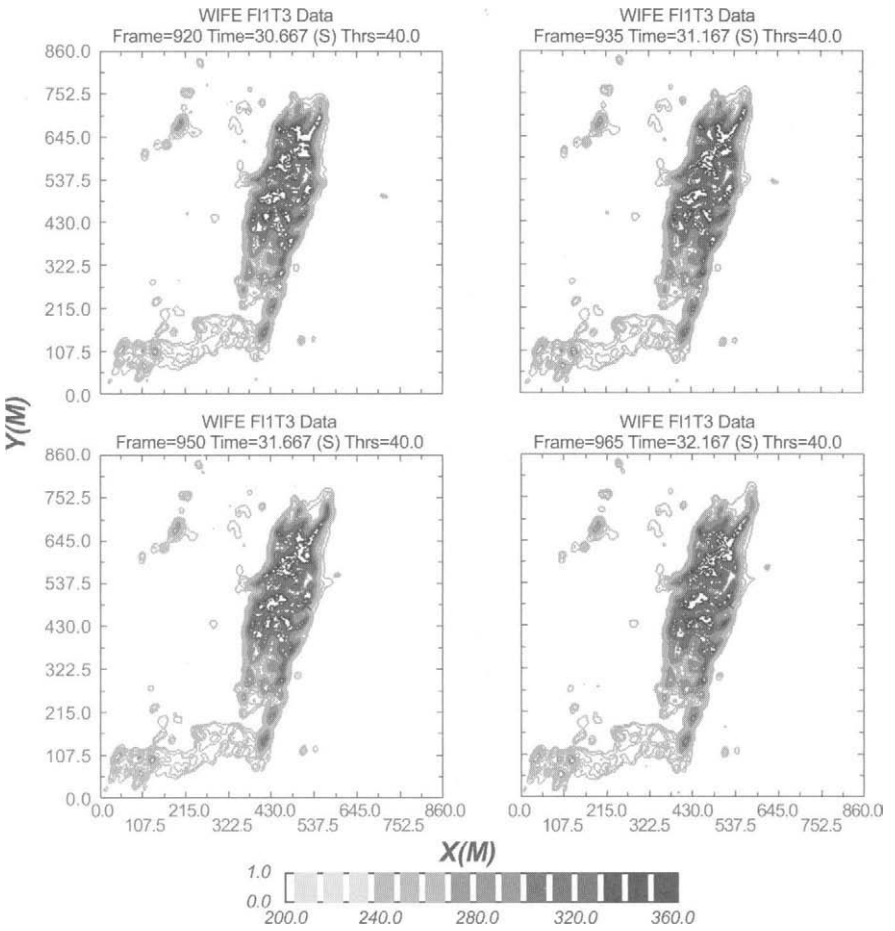

FIGURE 4 Airborne infrared imagery for fire spread analysis shows "hairpin" vortex (approximate location 753 m in y direction and 540 m in x direction) bursting forward at 70 m in 2 s. (After Radke *et al.*, 2000.)

needed to understand and predict fire behavior correctly. It is first necessary to define this feedback or coupling between the atmosphere and the fire.

In grass fires, it has been observed that the importance of wind speed diminishes after a critical speed is reached. Above certain speeds, further increases in wind speed do not stimulate additional increases in rate of spread or fire line intensity. To interpret this transition with increasing wind speed, Byram (1973) suggested a convective Froude number, F_{r_c}. The Froude number is defined as the ratio of the kinetic energy of the air and potential energy provided by the

fire. The measure of kinetic energy is the relative speed of the air passing over the fire, $U_0 = U - v_f$, where U is the ambient wind speed and v_f is the fire spread (i.e., rate of spread at the head of a fire). The measure of the potential energy used for the fire is the fire-line width in the mean wind direction times the buoyancy of the heated air. One possible formulation for F_{r_c} (Clark *et al.*, 1996a) is

$$F_{r_c}^2 \approx \frac{U_0^2}{g\dfrac{<\Delta T>}{T} W_f}$$

Here T is temperature and g is acceleration due to gravity. The $<\Delta T>$ is the average or mean value of the temperature anomaly ΔT over the region of intense heating and through W_f, the width of this region. Buoyancy is defined as $g(<\Delta T>/T)$. The Froude number is a nondimensional number. The values of U_0, W_f, T, and $<\Delta T>$ can therefore differ without the combination $U_0^2/[g(<\Delta T>/T)W_f]$ being different. Providing other governing parameters are also similar, we can expect the same behavior for flow with the same Froude number (i.e., all such flows are then dynamically similar).

An increasing F_{r_c} means that for increasing ambient wind speeds the fire deposits less heat into parcels of air as they move over the fire, until at some ambient wind speed the effect can be neglected. The process can be compared to a freight train of partly filled grain cars moving under a loading chute (Chandler *et al.*, 1983). If the train moves too slowly, the cars fill up and are unable to carry off as much grain as is being fed to them. Once the train reaches a speed at which the cars do not become filled, it is able to carry away all the grain, and an increase in speed will not change its ability to do so. To illustrate large F_{r_c}, simply run your hand over a burning match; when performed at comfortably high values of F_{r_c}, the interaction between hand and fire is negligible.

F_{r_c} can be used to gauge the level and type of coupling between the fire and atmosphere. The smaller the $F_{r_c}^2$, the larger the effect of buoyancy forcing on the acceleration of the flow. When $F_{r_c}^2 \approx 1$, the flow enters a regime where both fire and dynamics are important. When $F_{r_c}^2 < 1$, the flow responds strongly to the heating supplied by the fire, and the fire regime is plume-driven or convection dominated. If fire convection is to control the larger-scale dynamics, values of $F_{r_c}^2$ should be small. In high-wind-speed cases, as in wind-driven fires, $F_{r_c}^2 > 1$, and the flow is not dominated by the heating supplied by the fire. For typical values of $U_0 = U - v_f \approx 5\ \mathrm{m\ s^{-1}}$, $T \approx 300$ K, $\Delta T \approx 50$ K, and $W_f \approx 50$ m, the $F_c^2 \approx 0.3$. This implies that even for small, stable fires in weak or moderate winds, the effect of buoyancy forcing on the acceleration of the flow is significant, and the wind and fire are essential parts of the same system and cannot be separated. Also implied is that small F_c^2 is a necessary but not sufficient condition for severe coupled fire–atmosphere behavior.

IV. THE ELEMENTS OF FIRE MODELING

Regardless of the level of sophistication, current forest fire models require and provide, in one form or another, certain basic information. This includes initial total mass and dry mass of fuels (mass per unit area); initial moist/dry mass ratio of fuels; the rate at which fuel, once dry, burns (mass per unit area per unit time); the amount of energy provided per mass of dry fuel burnt; and the ratio of latent (moist) to sensible heat of this energy. The fire model outputs are sensible and moisture (latent) heat from the burning fuels (energy per second). Certain additions may be necessary: a percentage of the sensible heat provided by the fire dries the fuel; canopy ignition can occur when sensible heat flux from ground fuels exceeds a threshold value (energy per mass); to emulate smoldering, a random component can be added to the burn rates; and surface fuel is ignited by contact, where ignition contact follows the predicted fire spread rate and direction.

The ability to predict the rate of fire spread is recognized as the most important single requirement for successful fire suppression. Current models of forest fire spread assume that radiative heat transfer and convection, or wind, are the mechanisms that transmit heat from the flaming zone to adjacent fuels. Radiative heat transfer is increased by fuel changes that convert more of the reaction intensity into effective heat flux. Convection transfer is strengthened by increasing winds that can also increase both convective and radiant heat transfer. The important effects of terrain on fire propagation speed are also included.

There are many problems with current wildfire and fire spread rate models, but the major drawback is that, to apply them successfully, information on fuel, topography, and winds at the local, fire-scale level is required, information that is presently not available to fire managers and fighters. And because convection is a key mechanism for fire propagation after the incipient stage, knowledge of the small-scale atmospheric circulations in and around a wildfire is primary. In most applications, however, single values of wind speed and direction are applied over a large area and long time period. Therefore, microscale processes that affect the fire spread rate and involve the variable winds within the fire and adjacent fuel are not treated, whereas the formulae currently used to link the fire spread rate to the ambient winds ignore any feedback between the small-scale air motions and the fire. The solution to these deficiencies is to couple fire behavior and fire-spread-rate models to a dynamical atmospheric model.

V. MODELING THE ATMOSPHERE

To model the atmospheric circulation in and around a wildfire properly, a prognostic three-dimensional numerical model based on fundamental fluid

dynamics and capable of resolving convective-scale motions is required. A model of fundamental fluid dynamics consists of the Navier-Stokes equations of conservation of momentum, conservation of mass, and conservation of energy. Three dimensions are essential as fire dynamics are inherently three-dimensional due to advection, the solenoidal effect, vortex tilting, horizontal convergence, and turbulence or frictional drag.

The Navier-Stokes equations are smooth analytical functions, or differential equations, which in the case of conservation of momentum describes the instantaneous relation between position, velocity, and acceleration throughout the motion. A numerical model discretizes these differential equations to work at a finite number of regularly spaced locations called grid points. Each grid point holds the average value for a volume of surrounding air. This volume is called a grid cell or grid volume. To determine the functions at a future time, the equations are rearranged into forecast equations, and the functions are forecast for one-time step, utilizing present (and sometimes past) conditions to determine future conditions. Each operation in the analytical equations is expressed as a finite difference between grid variables. Computational time is spent for each grid point in the domain, and the computation is repeated for a succession of time steps in order to reach a forecast of possibly several hours duration. In a Cartesian coordinate system, the sizes of the grid cells in three directions are Δx (east–west), Δy (north–south), and Δz (vertical).

There are several sources of error in a numerical forecast. One is round-off error. The computer is able to store only a limited amount of information; as a result, real numbers are only approximated. Truncation is another source of error. An analytical variable is represented at a grid point as a function of its values at other grid points, the result being an infinite sum of terms, each of greater power of Δx or Δt (i.e., a Taylor's series expansion). For practical reasons, the computer retains the terms of the lowest power, the series is truncated, and higher power terms (which slightly improve accuracy) are neglected. Another error source is numerical instability, when the numerical solution rapidly diverges from the correct solution. Truncation is one cause, but numerical instability can also occur if the wind speeds are large, the grid size small, and the time step Δt not small enough. A necessary requirement for stability in the x direction with ambient wind speed U is

$$\Delta t \leq \frac{\Delta x}{U}$$

with similar requirements in the y and z directions.

A numerical model of the atmosphere–fire system must use, from an atmospheric scientist's perspective, a grid mesh with small Δx, Δy, and Δz values; currently typical sizes of grid cells in the domain of the fire can be tens of meters. Therefore, to preserve numerical stability, the time step must be also be

reduced. Typical time-step durations Δt are on the order of fractions of a second in the fire domain. A small time step has consequences for the total run time of the calculation and, since error is accumulated by the many more time steps required to reach a particular time, for the accuracy of the numerical solution.

The errors in initial conditions also affect the long-range predictability. The Navier-Stokes equations are nonlinear; as a result, the system is very sensitive to initial conditions. Such sensitivity means that a substantially different forecast can result from only slightly different initial conditions and that the forecast always becomes inaccurate with time. To minimize this error, initial conditions are specified as accurately as possible, and only short-term forecasts are considered trustworthy.

And lastly and most importantly, the physics of the fire–atmosphere system must be faithfully represented by the model formulation. The final source of error is then how accurately subgrid scale atmospheric and combustion processes are currently determined in terms of grid-scale (and therefore model forecasted) parameters. This is a central problem in numerical forecasting, and it is discussed further in the next section. Ideally the model framework should also be amenable to adding chemistry for pollution or smoke dispersal studies.

Because the computational demands of coupled atmosphere–fire modeling are great, additional features that diminish computational load while providing an accurate forecast are necessary.

One such feature is a vertically stretched, terrain-following coordinate system. In this system, the lower grid levels follow the contoured surface, while the vertically stretched coordinate allows a variable vertical resolution to the solutions of the equations near the surface and in regions of rough terrain.

Another such feature is two-way interactive grid nesting, also called grid refinement or multilevel grid nesting. Diverse scales of motion influence a wildfire's behavior, from the scale of the regional weather pattern (1000 km) down to the local and fire-generated flow (tens of meters and less), and multiple levels of interactive-grid refinement allow the numerical model to run over such a large range of scales. A large outer domain with large-sized grid cells and time steps, and initialized with coarse resolution meteorological data from, say, General Circulation Forecast Models, determine satisfactorily the largest scale atmospheric circulation. Inside or nested in this domain are successively smaller and smaller domains, each containing topography at the grid resolution of that domain, while fields are matched between the boundaries of the coarser grid and finer grid domains. Eventually the meteorology is forecast in the smallest domain, where fine-scale grid cells are used to resolve the fire's convective-scale motions.

A further refinement is an adaptive grid mesh in which the finite difference grid is refined in selected regions that may be changed in time to follow evolving features such as the moving fire front.

As in Section II, the description of a three-dimensional numerical atmospheric prediction model presented is purposely simplified to convey the essence of the approach. Although there are many more aspects involved, they are beyond the scope of this text and are therefore not included.

VI. THE COUPLED FIRE–ATMOSPHERE MODELING APPROACH

We have seen that even for small, stable fires coupling between the fire and the atmosphere can be significant. Temperature, humidity, and wind fields are noticeably altered by the fire, which in turn alter the fire. Once temperature and humidity fields are altered, pressure gradient and buoyancy forces come into play, and the velocity field changes. Velocity field changes affect fire behavior and fire spread rates, which can advance the fire front, igniting more fuel, releasing sensible and latent heat, and repeating the process.

The coupling between the fire and the atmosphere occurs mainly through the fluxes of sensible and latent heat from the ground fuel and canopy burns. Radiation is also important, both in preheating the fuels ahead of the fire and shortening their ignition time and to the atmospheric circulation in and above a wildfire. To couple current fire and numerical atmospheric prediction models, radiation and sensible heat and moisture fluxes associated with the fire are included as subgrid-scale sources of heat in the atmospheric model's conservation of energy equation. Wind is also modified by the forest, especially the vertical wind profile, and the effect of surface and forest canopy drag on the velocity field is a subgrid-scale momentum source in the atmospheric model's conservation of momentum equation.

The heat fluxes and radiation from the fire are absorbed by the air, and a method for incorporating this effect in the atmospheric model is required. A very simple approximation is that the amount of radiation absorbed into the atmosphere decays exponentially with height, where the depth of extinction may range from 50 to 100 m in the vertical. In reality, the interaction between radiation and the atmosphere is much more complex than this and is not well understood. For example, an accurate treatment of flame front radiation onto unburned fuel and resulting fire spread strongly depends on a good knowledge of the vortex dynamics at the fire line. To understand the impact of radiation on fire spread, rotors produced by the mechanism of enhanced vortex tilting might be approximated as a radiating vertical wall of flame, whereas the forward bursts of flames in hairpin vortices cannot be reasonably approximated in this way. To date, this type of interaction has not been taken into account.

Yet, however they are handled, the effects of convection, turbulent mixing and frictional drag, and black body radiation occurring on scales not resolved by the numerical atmospheric model must be represented accurately.

Because current wildfire formulae are mainly algebraic and based on statistical or empirical ideas and do not describe the microscale processes that affect the fire spread rate and involve the variable winds within the fire and adjacent fuel realistically, coupling the fire model with the atmospheric model cannot completely accomplish the task of including the feedback between the small-scale air motions and the fire. The solution is to develop a physically based, dynamic wildfire model. Yet, even if a fully physically based wildfire model were available to couple with a fully physically based atmospheric model, the technical and conceptual difficulties to be overcome are tremendous.

Within fires, there are small vortical structures on the millimeter scale that tightly bend the flame fronts, up to vortex structures on length scales of many meters. The time scales range from milliseconds in submillimeter eddies to the puffing frequencies on the order of seconds. In addition to these fire-convective length and time scales are diffusive length and time scales, from the submillimeter and submillisecond range required for resolution of chemical species diffusion gradients in flame zones, to the tens of meters and thousands of seconds required to resolve the length and time scales of fire/object interaction. More than five orders of magnitude in temporal and spatial resolution are required to simulate directly all the relevant scales within the fire. Coupling a numerical fire simulation with a numerical atmospheric model adds a further five or more orders of magnitude in resolution when attempting to incorporate atmospheric forcing by meteorological conditions on the regional weather scale.

Given the present level of computational resources, no numerical simulation tool is capable of simultaneously resolving all required length and time scales associated with forest fire phenomena. The problem is easily illustrated by considering the following: A numerical model basically divides three-dimensional space into grid cells with volume $\sim(\Delta x)^3$, and the computations will locate a moving fluid particle within one of these cubes. If greater resolution and accuracy are desired, a finer mesh with smaller grid cells is used. To improve the accuracy tenfold for instance, the size of the grid cell must be $\Delta x/10$ instead of Δx. There are $10^3 = 1000$ such small cubes in a single large one, all of which must be allocated some place in the memory of the computer. This means that the computations which can trace a parcel's location within 100 m in 1 s will run for almost 20 minutes to pinpoint the same trajectory within 10 m. By this time, of course, the model forecast can be meaningless, the parcel having in reality long since left the computed position. Alternatively, to find the answer within 1 s, some way must be found to perform the same computations 1000 times faster, which cannot be achieved by technological means only. Today, speed increases tenfold, not a thousandfold, from one generation of computers to the next. (The current observation is that computer speed and memory capacity double about every 18 months.) This problem is not specific to coupled fire–atmosphere modeling; in every area of science, there are a great many computations that cannot be performed now or in any foreseeable future.

Basically there are two approaches to dealing with the numerical modeling of phenomena operating on a large range of scales. One is starting with the smallest length scales and resolving all the physical processes up to the largest length scales that can be computed. The other is starting with the largest length scales and resolving downscale with as many grid cells that can be computed. Although the first approach is preferable from a scientific perspective, the largest length scales within a fire model that currently can be numerically modeled are on the order of centimeters. Even with the tremendous growth in both speed and memory for computing hardware, this approach will likely be limited to length scales significantly smaller than the resolution of the smallest grid used by coupled atmosphere–fire models. The second approach uses a technique known in the atmospheric science community as subgrid-scale parameterization. Physical mechanisms with length and time scales below the minimum that can be resolved by numerical models are expressed either empirically or mathematically in terms of observed variables or model forecasted parameters in an ad hoc attempt to represent the physical phenomena as realistically as possible. Subgrid-scale parameterization is not specific to atmospheric numerical modeling; this is also the technique used by combustion scientists to model turbulence in the flow, combustion processes, soot formation, and thermal radiation of combustion products in a fire, along with the turbulent eddy viscosity or friction near solid surfaces. Attempts are made to develop transport models that connect fire propagation rates to the full conservation equations of energy, momentum, species concentrations, mass, and turbulence and that represent the essence of a combination of many microscale processes without resolving each process in complete detail (Linn, 1997). In both atmospheric and fire combustion numerical modeling research, subgrid-scale parameterizations have proven to represent successfully many unresolved physical processes in the system to the degree that is needed, and the development of and improvements to parameterizations are ongoing efforts.

A. The Importance of Ignition Tracing on Fire–Atmosphere Coupling

One major technical difficulty with a coupled fire–atmosphere model is ignition tracing. In a numerical model, the fuel is necessarily divided into grids. The simplest way to advance the fire through the fuel grid mesh is to ignite entire fuel cells on contact. For example, four tracers are assigned to a grid cell once the ground fuel for that particular cell is ignited. Based on the prescribed spread rate, the tracers move parallel with and against, and normal right and left of, the tracer-advecting wind. Once a ground tracer reaches an unburned grid box, that fuel cell is ignited, and four new tracers are initiated at the point

of contact. Tracers should not move into burned out or burning grid boxes. One of the immediate problems with this approach is that ignition tracers do not necessarily maintain or move to increase the fire perimeter within a fuel box, and negative distances can be covered. This happens when the local fire convection changes the wind direction, and an ignition tracer that was moving with the wind suddenly finds itself in an opposing wind condition. With this simple approach to ignition parameterization, it is difficult to prevent the model ignition tracer moving back into burned or burning regions within a fuel grid cell. Obviously this simple ignition parameterization fails to maintain or move the ignition pattern to increase the fire perimeter within a fuel box in a realistic fashion.

Another result of this simple approach to ignition is that the problems of grid mesh size are exacerbated. Model resolution is always an issue, but it is especially so for the fire–atmosphere system where model resolution has an extremely important influence on heat transport away from the fire. When the entire fuel cell is allowed to ignite on contact and the model resolution is too coarse, the model fluid becomes inefficient at transporting heat, artificially changing the heat balance.

When the fire begins, there is initially no convection to remove heat efficiently, causing very high air temperatures to build near the surface. Once the convection is well established, the temperature equilibrates to significantly lower values as the convective heat transport balances the heat flux from the fire. The time the fire takes to establish this balance in a numerical simulation using a 20-m grid resolution is approximately 1–2 minutes. After convective adjustment, the atmosphere transports heat away from the fire such that the convection is in balance with its heat source. The sensible heat flux into the atmosphere is calculated as

$$F_s = c_p <\rho w' T'>$$

where c_p is the specific heat capacity at constant pressure p, ρ is air density, and w' and T' are the respective vertical velocity and temperature perturbations or fluctuations from the mean. The $< >$ denotes the average or mean value over the region of intense heating. When using a 20-m grid resolution, realistic numerical model values for the maximum vertical velocity anomaly Δw are approximately 20–30 m s^{-1}, and for the maximum temperature anomaly ΔT are approximately 40–80 K over the region of intense heating. A rough estimate of F_s supplied by these model perturbations is, therefore,

$$F_s \approx c_p <\rho \Delta w \Delta T> \approx 0.8 \text{ to } 2.4 \text{ MW m}^{-2} \quad (1)$$

which easily accounts for the ~0.8 MW m^{-2} of sensible heat flux typically emitted by the fire. ΔT is limited to values as low as 40–80 K in a forest fire due to the efficient heat transport by convection, even though the flames may have radiant temperatures of ~800–1600 K.

To establish a horizontal fire resolution when the entire fuel cell ignites on contact, take $\Delta x_{fuel} \leq v_f \tau$, where τ is the time it takes the fire to burn the small fuel, and v_f is the fire spread rate. A fire line typically moves 10–25 m in time τ. For $v_f \approx 0.5$ m s^{-1} and $\tau \approx 50$ s, $\Delta x_{fuel} \leq 25$ m should provide a continuous fire behavior. If Δx_{fuel} is too large, the heat flux from the fire is discontinuous, which forces air to always readjust to the fire as it moves through the fuel grid mesh. Because the convective adjustment time is comparable to the time required for the small fuel to burn, namely about 100 s, the effects of the heat flux from a model with coarse fuel resolution will not average out with time. A $\Delta x_{fuel} = 10$ m horizontal resolution for the fire is generally sufficient to avoid discontinuities in the numerical model solutions when the entire fuel cell ignites on contact. This relatively small grid cell necessarily increases the computational load.

If horizontal and vertical resolutions in the atmospheric model are substantially reduced, then the heat flux is input into the model atmosphere in an unrealistic fashion, and the model fluid becomes inefficient at transporting heat. The numerical results are much higher temperature fluctuations and a much smaller convective Froude number. An almost immediate model blowup fire with uncontrollable fire spread rates in excess of 50 m s^{-1} can occur. The ignition parameterization and resolution must not dictate the values of F_s and F_{r_c}, and thereby the overall fire behavior.

An effective tracer ignition parameterization is instead where the subgrid-scale ignition pattern moves through each fuel cell at the fire spread rate directed by the fire-scale winds. What is needed and what has been recently developed is an improved tracer ignition parameterization in which the coordinates of ignition tracers define a particular burn area within the cell. These coordinates are time dependent and allow fires of arbitrary orientation and shape to move through a mesh of fuel grids at fire spread rates, with minimal adverse effects on the model that result when the entire fuel cell is allowed to ignite on contact. This type of ignition parameterization provides spatially smooth predictions of heat and moisture fluxes from the fire and can perform at higher grid resolutions. Larger grid mesh values can be used with this ignition approach, although it is still necessary to consider the influence of model resolution on heat transport away from the fire, and to resolving the fine-scale convective processes that maintain or move the ignition pattern to increase the fire perimeter within a fuel box in a realistic fashion.

Figure 5 shows an example of this type of tracer ignition for a spot fire expanding outward under zero wind conditions. The plot shows a region of 21-by-21 fuel cells with the solid circular contour outlining the fire line. The insert shows the regularly shaped fire line constructed from the shapes provided by four ignition tracers within each fuel cell nearest the fire line. Most of the fuel cells inside the fire line are fully ignited except for those near the fire line which are only partially ignited.

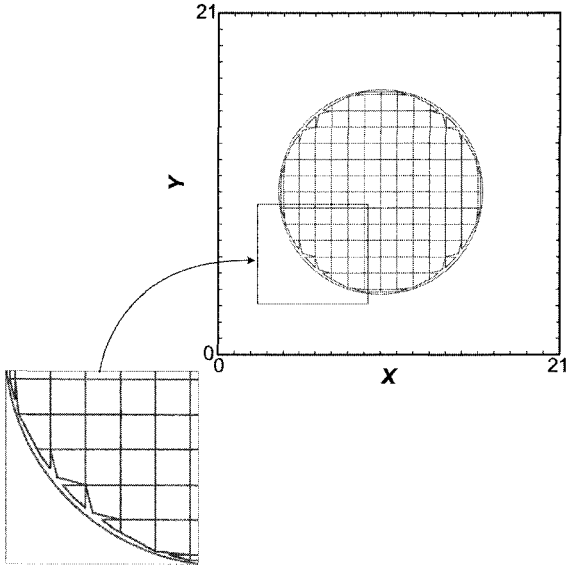

FIGURE 5 Circular-shaped fire line simulated for a spot fire in zero wind. The circular solid contour represents the fire line, and the interior rectangles represent the individual burnt or burning fuel cells. See text for explanation.

VII. IDEALIZED STUDIES OF WILDFIRE BEHAVIOR

Despite the difficulties to overcome, efforts at numerical coupled atmosphere–fire modeling are currently helping to improve our understanding of wildfire behavior and will in the future predict it. In the following we describe the numerical results from model simulations of Clark *et al.* (1996a,b) and Coen *et al.* (1998). Their simulations produced a number of realistic features of natural fires. These include the bowing of fire lines into conical shapes, the formation of fire whirls that touch down within the fire line and break it apart, microscale vortices in the fire line that strongly accelerate the local winds and fire spread rate, how negative vertical wind shear can contribute to extreme fire behavior, and the deflection along the ridge of a line fire propagating up a relatively sharp slope. We also describe the numerical results from model simulations by Bossert *et al.* (2000) and Linn *et al.* (2000). Their simulations demonstrate the sensitivity of fire behavior to different fuel characteristics and configuration. The dependent fuel parameters studied were fuel load, moisture, and type, and a two-storey fuel canopy. We discuss the use of the infrared video camera, a remote sensing device that provides high spatial and temporal observational data of wildfire winds and heat fluxes.

A. Fire-Scale Convection Drawing the Fire Line

The perimeter of a moving fire line normally does not spread evenly, but with a bias. The center spreads slightly more rapidly than the ends; a line of fire narrows and forms a head. In moderate ambient winds, prescribed burns ignited in a line almost always develop a parabolic shape to the fire front. This feature occurred in Clark *et al.* (1996a,b), in a series of idealized numerical experiments designed to test the effect of different constant background winds on the evolution of a short ($\approx$ 400-m-long) fire line.

In weak ambient winds (< 3 m s^{-1}), the model results show a chaotic and broken fire front. Under these conditions, air feeding the hot convection column comes directly from below. The vorticity dynamics described in Section VII.B (and Appendix II) produce vertical vortices embedded in the fire line, and the erratic fire-scale, fire-generated winds break up the fire line.

Under moderate ambient wind conditions ($\approx$ 3 to 5 m s^{-1}), numerical simulations produce a stable fire line, where moderate winds move the mean surface effects of convection ahead of the fire line. The convection cell aloft remains just downstream of the fire, drawing the fire with it, and its near-surface convergence pattern induces a smoothly, continually evolving, parabolic shape to the fire line. Figure 6a shows the evolution of a fire line in a constant background or ambient wind of 3 m s^{-1}. Figure 6b shows that a slightly faster constant ambient wind speed of 5 m s^{-1} accentuates this effect. This convective feedback is a linear fire-scale phenomenon, in that smaller scale interactions between developed flow do occur, but the overall effect remains.

Once a fire line is long enough, it cannot sustain a single convective updraft column. The essentially two-dimensional updraft along a linear fire line experiences along-line roll instabilities that can cause the line to break into multiple convective updrafts or towers. Providing conditions similar to those required to form the local parabolic shape exist, multiple protrusions or fire heads form.

An example of this (Figure 7) occurred in the 1985 Onion fire in Owens Valley of California (C. George, personal communication). The fire line developed protrusions or fingers that were spaced about 1 km apart and that appeared only with an ambient wind. When the mean wind died down, the fuel between the fingers burned out, forming a more linear and stalled smoldering fire line. With the return of the wind, fire spread resumed with fingers reforming. Numerical simulations with a coupled atmosphere–fire model reproduce this phenomenon. Modeling results show one convective finger developing along an initially 400-m fire length and two convective fingers along an 800-m fire line.

These simulations demonstrate a useful aspect of a numerically coupled atmosphere–fire model: the ability to examine the effect of a single variable on the fire behavior. In these experiments only the background wind was changed.

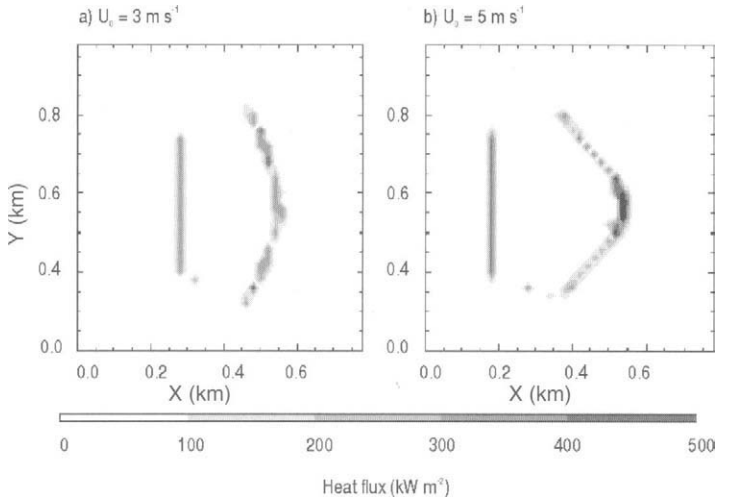

FIGURE 6 Numerical simulations of a fire line (heat fluxes greater than 0.1 MW m^{-2}) in constant background winds of (a) $U_0 = 3$ m s^{-1} and (b) $U_0 = 5$ m s^{-1}. (After Clark *et al.*, 1996a.) The bottom left to right axis is the x axis, the vertical axis on the left is the y axis, and units of x, y are km. The straight line parallel to the y axis is the initial fire line.

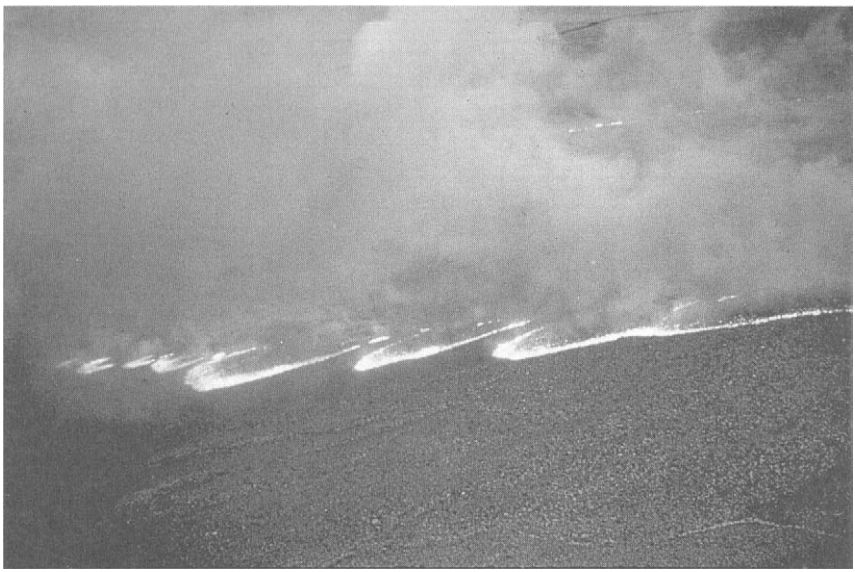

FIGURE 7 The 1985 Onion sage brush fire in Owens Valley, California. See text for description. (Courtesy of C. George, USDA Forest Service, Intermountain Research Station, Missoula, Montana.)

Other ambient meteorological conditions were set to neutral. No topography, Coriolis force (deflection of moving air by rotation of the Earth), or diurnal effects were included. The fuel was homogeneous so that any scale selection or breakup in fields and fire line were due to the dynamic and thermodynamic interactions between the fire model and the meteorology. Different fuel properties had been suggested as being responsible for the fingering fire behavior shown in Figure 7. The simulations show that the ambient wind strength, not the properties of the fuel complex, was responsible for the differences in fire line behavior.

B. Fire-Scale Vortices Disrupt the Fire Line

In prevailing winds, the leeward side of the convection column is a preferential spot for the development of tornadic fire whirls and, under the right wind conditions, these fire-scale vortices can disrupt the fire line. Clark *et al.* (1996b) set up numerical experiments to test the effect on a short (400-m-long) fire line of the change in ambient wind speed with height. Two ambient wind profiles were used (Figure 8), one a constant westerly wind (3 m s^{-1}), the other a hyper-

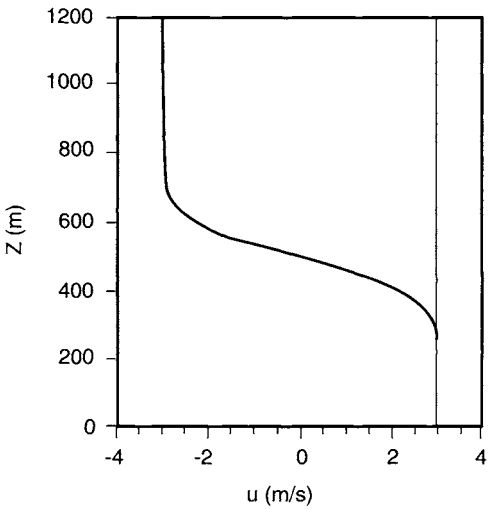

FIGURE 8 Two idealized wind profiles used to demonstrate fire behavior caused by coupling between convective motions and ambient vertical winds. See text for explanation.

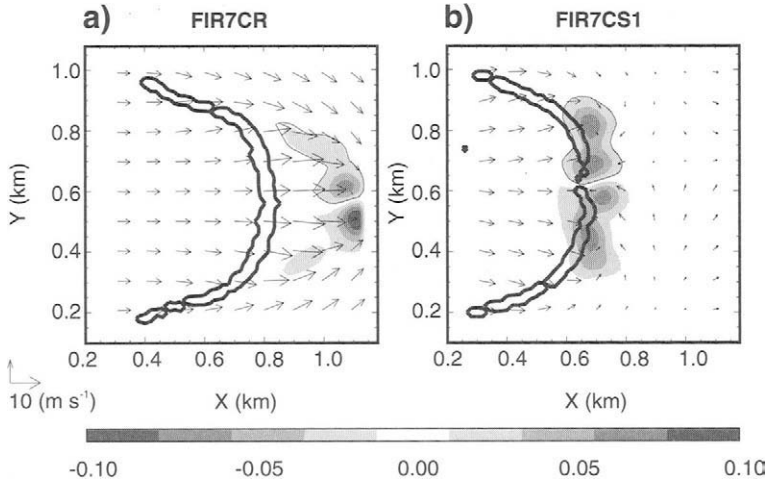

FIGURE 9 Fire lines (solid outlines of heat fluxes greater than 0.1 MW m^{-2}) and vertical vorticity (shading) are shown for (a) the constant wind and (b) the hyperbolic tangent wind profiles in Figure 8. Vectors denote local winds at 15 m above ground level. (After Clark *et al.*, 1996b.)

bolic tangent profile westerly (3 m s^{-1}) at the surface, decreasing with height to 500 m above the ground, and then reversing direction to an easterly wind (-3 m s^{-1}) aloft.

Figure 9 shows the near-surface vorticity patterns and fire line ignitions for the two experiments. The constant ambient wind profile case develops a parabolic fire line shape as described in Section VII.A, whereas the hyperbolic tangent profile case shows a fire line separated at its center.

Both cases produced a counterclockwise rotating vortex ahead of the fire line and south of the updraft core and a clockwise rotating vortex ahead of the fire line and north of the updraft core. The rotating vortices are the result of tilting the horizontal shear in the convection into the vertical by the fire's central updraft core, the process that is depicted in Figure 1.

In the constant ambient wind profile, the vortices, once developed, touch down, but well in front of the fire line. In the hyperbolic wind profile, the vortices develop in front of the fire line, but eventually the winds above 500 m advect the vortices back into the fire line, where they touch down in the fire. The counterrotating winds are sufficient to overcome the ambient winds, causing reversed flow and breaking of the fire line. The mathematical explanation for this development is given in Appendix II. Although the effect of vorticity dynamics on the fire line propagation is obvious, there is no evidence from the

numerical results that the events in the second wind profile case weakened the fire more than the first.

C. Microscale Vortices Affecting Fire Spread

The smallest scale vorticity at the fire front is important to the dynamics of fire spread. Tilting into the vertical of the small-scale negative shear (wind speeds decreasing with height) close to the surface provides increased winds in the direction of the fire spread. This is the situation depicted in Figure 1 and can result in a marked increase in the rate of fire spread (as illustrated by the right-pointing arrow in Figure 1b). It is simple for a numerical model to determine when and where in the fire domain maximum fire spread rates are. The strongest fire spread rates occurred for the second wind profile simulation (i.e., Figure 8 and Figure 9b), and the sequence of events was tracked by the numerical model.

The vorticity advected back into the fire and behind the fire line when the easterly wind aloft interacted with the fire; as a result, chaotic and amplified fire behavior set in at about 16 minutes into the simulation. Figure 10 shows a time sequence of vertical velocity after the amplified behavior set in. A fire-induced downdraft in the rear flow produced near-surface vertical shear that moved through the fire front, adjacent to an existing vertical rotor. Vertical tilting of this shear by local updrafts intensified the rotation rate of vertical rotor leading to anomalously large fire spread rate v_f values. The vertical wind increased to well over 5 m s^{-1} at 15 m above ground level. Model wind speeds are necessarily averaged over a large grid volume (20 m on a side in this case). Unlike model winds, tornadic whirls at 10–50 m in diameter in real fires obtain updrafts and horizontal velocities of 50–100 m s^{-1}.

D. The Effect of Atmospheric Stability and Wind Changing with Height on a Fire Propagating over a Small Hill

Observations, laboratory experiments (Weiss and Biging, 1996), and computer models (Linn, 1997; Coen *et al.*, 1998) show that when fire spreads on sloped terrain, it spreads faster uphill on steeper slopes. This is due to a combination of dynamic effects, the relative importance of each still being debated (Baines, 1990). One effect is that the fire's convection increases momentum and wind velocities near the ground. Another involves the fluid dynamics of flow over

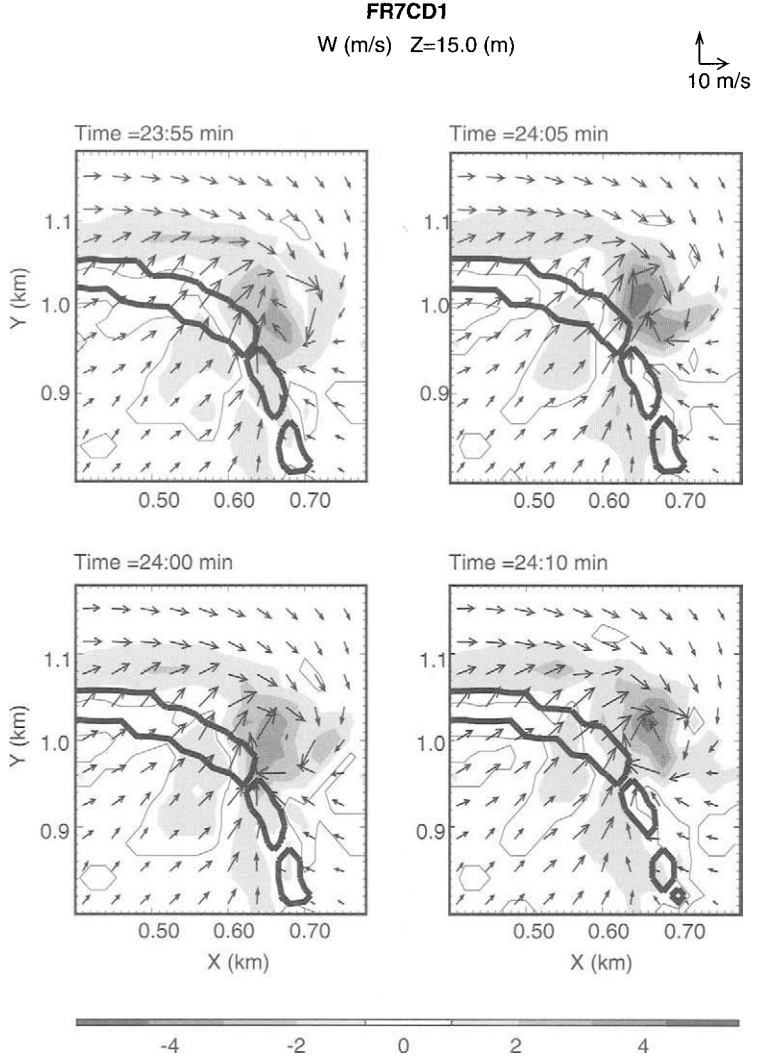

FIGURE 10 The vertical velocity (units m s^{-1}) from a numerical simulation of an initially 400-km-long fire line in a hyperbolic tangent wind profile where $U_0 = \pm 3$ m s^{-1}. See text for explanation. Four times are shown and frames are 5 s apart. Solid outlines are for heat fluxes greater than 0.1 MW m^{-2}. Vectors denote local winds at 15 m above ground level. (After Clark *et al.*, 1996b.)

hills, which leads to accelerations and decelerations in wind velocities even without the presence of a fire. A third effect is attributed to radiation and convection preheating and drying the fuel ahead of the fire (Rothermel, 1972) and to flames being brought closer to the fuel and propagating the fire by contact.

Figure 11 presents the results of an idealized simulation by Coen *et al.* (1998) of a fire line propagating over a small Gaussian-shaped ridge with a relatively sharp slope (height 200 m and half-width 300 m) and extending north–south over the entire model domain. The hyperbolic tangent wind profile of Figure 8 was again used, but with stable atmospheric conditions below 500 m and un-

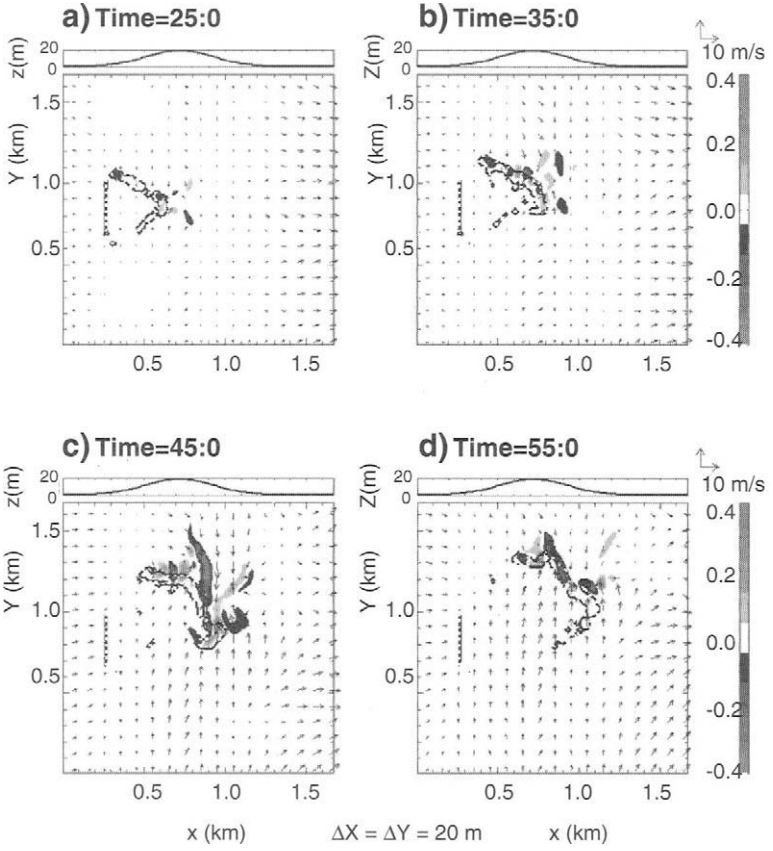

FIGURE 11 A near-surface horizontal cross section of the vertical vorticity (shaded) associated with a fire line (solid outline of heat fluxes greater than 0.1 MW m^{-2}) as it flows over a small ridge at 25, 35, 45, and 55 minutes into the simulation. Ambient atmospheric conditions are a 3 m s^{-1} low-level, westerly (from the left), stable flow. The vectors indicate the winds at the 15 m height. The west–east profile of the hill is shown above the main figure.

stable above.[1] These simulations demonstrated the unusual interactions that occur between a fire and its atmospheric environment when spreading over mountainous terrain for the chosen atmospheric conditions. Figure 11 shows that, as the fire moved up the slope, the right flank weakened and died, and then, instead of continuing to propagate down the other side, the left flank veered sharply along the ridge line. Since the flow driving the fire forward was symmetrical and cannot be the source of asymmetry, this fire behavior suggests that an instability amplified some small asymmetric disturbance.

After bowing forward into the expected bow-shaped fire line (Figure 11, time = 25 min), other interesting features appeared in this simulation. These included a large fire-scale rotation just in the lee of the ridge (Figure 11, time = 45 min), into which flowed a string of vertical vortices with alternating sign that formed initially at the rear edge of the active (left) flank of the fire.

The atmospheric situation for the simulation shown in Figure 11 is depicting a type of air flow known as nocturnal drainage flow. At night, air cools. Cold air is heavier than warm and can flow downslope with speeds of 3 to 20 m s^{-1}. These flows are characterized by a shallow, stable layer of cool air spreading quickly near the surface under a layer of less stably stratified air that is either still or traveling in the opposite direction. Figure 11 demonstrates how complex the interactions between the fire and the atmosphere can become even for common atmospheric flows like low-humidity, nocturnal drainage flows. The results of this simulation also raise a crucial question: the possible impossibility of predicting fire behavior when a sudden amplification of small, transient instabilities in the flow leads to such deviant behavior.

E. Sensitivity of Fire Behavior to Fuel Characteristics and Configuration

A method for creating a more general operational atmosphere–fire model is to use a physics, as opposed to empirically, based fire transport and behavior model to represent the processes of forest fire combustion and spread rate. One such model is the FIRETEC (Linn, 1997; Linn and Harlow, 1998). The FIRETEC is based on conservation of mass, momentum, species, and energy. It includes a

[1] Whether an atmosphere at a location is stable or not depends on the resulting motion of a parcel of air that is displaced vertically from its initial position. If the parcel moves further away from its initial position, then the atmosphere is unstable and convection occurs; if the parcel returns toward its initial position, then the atmosphere is stable; and if the parcel does not move once displaced, then the atmosphere is neutral. The magnitude of the parcel's vertical acceleration is determined primarily by the temperature or density difference between the air parcel and its environment at a given location, time, and pressure level.

representation of fuel pyrolysis, turbulent transport of combustion products, and radiative preheating of fuel due to the approaching flame front.

The FIRETEC has been coupled with the HIGRAD, an atmospheric dynamics model developed to handle the sharp temperature and flow gradients encountered in the vicinity of a wildfire (Reisner *et al.*, 1998, 2000). Using FIRETEC/HIGRAD, Bossert *et al.* (2000) simulated a small portion of a 16,000-acre fire in steep terrain (Calabasas fire, October 21 to 22, 1996, Corral Canyon, CA). FIRETEC allows a fully three-dimensional characterization of fuel, and in this study the dependent fuel parameters were fuel load, moisture, and type. The results show how the fire responded to four different fuel types. Even though the fuel load and moisture contents were variable among the four fuel types, the numerical results were not dramatically different in three of the four cases. In contrast, one fuel type, which had the lightest fuel load and highest moisture content, produced radically different fire behavior. The fire never achieved sufficiently high enough temperatures to sustain itself up the sloped terrain and died after 8 minutes of simulation. This result shows that the FIRETEC model is sensitive to the specification of fuel load and moisture. Bossert *et al.* (2000) also produced one simulation showing steeper topography overwhelming any detailed specification of fuels, resulting in an equivalent of a blowup fire. Convective heating of a steeper portion of the slope by hot gases from the fire's plume caused the entire portion of the slope to be engulfed by fire after only one additional minute of simulated time.

FIRETEC was also used to consider multistorey fuel canopies involving ground and crown fuels. Linn *et al.* (2000) show FIRETEC/HIGRAD simulations of fire sensitivity to live moisture in the canopy fuel; as expected and in agreement with observations, high moisture in the canopy fuel and the fire was confined to surface; low moisture in the canopy fuel and the fire crowned. These results demonstrate the potential of using a physics-based fire behavior model coupled with an atmospheric prediction model for exploring such phenomena as crowning. Linn *et al.* (2000) also simulated a grass fire in which FIRETEC/HIGRAD caused irregular fuel consumption that produced a nonhomogeneous fire front and burn pattern. The simulated burn pattern (Figure 12) is similar to patterns sometimes observed in real fires: streaks of burned and unburned fuel, perpendicular to the fire front and parallel to the ambient wind.

VIII. INFRARED OBSERVATIONS OF FIRES

There is no substitute for direct observations of fire dynamics and behavior. Unfortunately severe fires are almost inaccessible to planned observations, and forestry researchers are required to build their models on sometimes shaky ob-

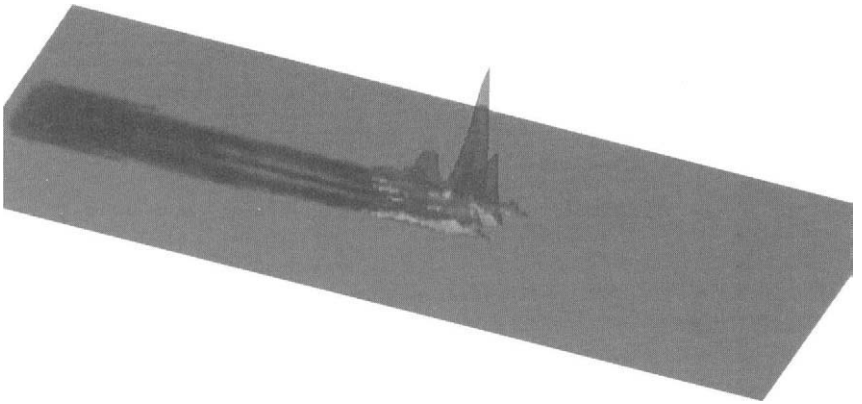

FIGURE 12 Side view image of a three-dimensional simulation of a tall-grass fire in 4 m s^{-1} ambient winds blowing perpendicular to the fire front. (After Linn *et al.*, 2000.)

servational foundations. Theoretical descriptions of convection patterns and behavior in fires still rely heavily on laboratory and computer simulations. This is changing. Advances in understanding come from the application of remote sensing instrumentation. It is now possible to probe fires from a safe distance with Doppler radar and lidar, and most recently, infrared or IR video.

Although data describing the fire spread rate and some qualitative aspects of wildfire behavior exist, none has revealed the very small convective time and spatial scales in the fire. The intense vortices of various strengths and sizes in fires have been observed both experimentally (Church *et al.*, 1980) and in model simulations (Heilman, 1992; Heilman and Fast, 1992; Clark *et al.*, 1996a,b). As discussed in the introduction, observations in one case study (McRae and Flannigan, 1990) show that fire vortices can rip out and loft standing trees. A pool fire simulation produced counterrotating vortices to characterize the structure of rising smoke (McGrattan *et al.*, 1996). Similar vortices were observed in fires using lidar and radar where the scale of the observed vortices was on the order of 100 m (Banta *et al.*, 1992).

The fire convection is rarely more than a few meters, lasting rarely more than a split second. It is necessary to observe fire-scale features on time scales of 0.05–0.1 s and spatial scales of 1–3 m. The long dwell time, the low scanning rate, and the spatial resolution of the Doppler radar (~10 μm) and lidar (~3 mm) do not provide wind speed measurements on such small scales (Banta *et al.*, 1992).

However, current IR camera capability provides high-frequency (1/30 s) and high resolution (0.05–0.16 m) radiant temperature images that are being used

to derive wind fields to provide clues to motions on scales of the order of meters and time scales of fractions of a second. Infrared video cameras have a temperature measurement accuracy of better than $\pm 2°C$ at temperatures up to 2000°C and can resolve temperature differences of less than 0.1°C. The IR camera views a shallow depth into the flame front and variabilities in the distribution of hot soot particles provide the information necessary to derive two-dimensional images of flow. Analysis of these images provides estimates of velocities in the vertical and in one horizontal direction. Measurements in crown fires in the Canadian Northwest Territories suggest updrafts of 10 to 30 m s^{-1}, downdrafts of -10 to -20 m s^{-1}, and horizontal motions of 5 to 15 m s^{-1} throughout the fire (Clark *et al.*, 1999).

IR temperatures and vertical winds are used to estimate sensible heat fluxes from the fire. Following Eq. (1), the sensible heat flux is

$$F_s \approx c_p <\rho w(T_{IR} - \overline{T}_{IR})> \tag{2}$$

where w is the vertical velocity at the location of IR temperature measurement T_{IR}, and $\overline{T}_{IR}$ is the time and area average of T_{IR}. Heat fluxes calculated according to Eq. (2) then can be compared with expected values based on fuel loading and observed burnout times to corroborate the image flow analysis.

It is possible to infer from an IR image flow analysis a number of physical mechanisms contributing to the fire spread rate. IR camera imagery appears to represent such fine-scale fire structures as hairpin vortices or turbulent bursts and the tilting of horizontal vortices leading to counter rotating convective towers where the estimated vertical vorticity is 4–10 s^{-1} (Clark *et al.*, 1999). These fire structures determined by IR video measurements are being compared to and used to corroborate computer simulations such as those described in the previous section.

IX. CONCLUSIONS AND FUTURE WORK

In this chapter, we describe the coupling of an atmospheric prediction model with an empirical fire spread model so that the fire–atmosphere is treated as a single, dynamic system. This is a fairly recent and major advance in the modeling of wildfires. Unlike the wildfire models that have traditionally been used to assess the risk, behavior, and spread of fires, this model is capable of simulating the convective-scale fire–atmosphere circulations, including the small-scale vortex dynamics, that play an important role in influencing a wildfire's overall behavior, as well as fire spread rates. And unlike traditional wildfire models, the coupled fire–atmosphere modeling approach can include the possible impacts of evolving large-scale atmospheric forcing on the fire and vice versa.

There are two major problems to overcome before this approach can be used to predict forest fire behavior. First, we must learn to faithfully represent the physics of the fire–atmosphere system to the degree that is needed. Second, we must develop observational systems and techniques to provide the detailed observations of fire structures that are required to improve and validate the numerical results of the fire–atmosphere model. Real-time simulations of wildfire events may be possible in the near future using newer computer technology, provided also that topography, initial weather data, and fuel data can be gathered quickly for use in the model, and new visualization techniques be developed to display results in real time.

We have discussed a few numerical modeling results from publications (Clark *et al.*, 1996a,b; Coen *et al.*, 1998; Bossert *et al.*, 2000; Linn *et al.*, 2000) directed at improving our understanding of wildfire behavior. To gather the observations to validate numerical model results from simulations like these, we have briefly described the measurement technique of infrared video imagery. The current analysis of IR video imagery is capable of estimating two-dimensional wind fields and heat fluxes from the fire.

One weakness of the coupled fire–atmosphere modeling approach is the currently necessary employment of empirical formulae for forest fire models. The accuracy of ignition spread is dependent on the fire spread rate model, while the heat and moisture fluxes absorbed by the air are dependent on the accuracy of the fire model. Eventually forest fire models and fire spread-rate formulae must be replaced with more physics-based treatments of microscale processes within the fire and adjacent fuel. This is an extremely difficult exercise. Forest fires have complicated chemistry, radiation, and combustion properties. The interactions between forest fires and air flow are highly nonlinear. Diverse scales of motion influence a wildfire, and at almost every scale the physics require fully dimensional temporal and spatial dynamics.

The ultimate goal is to develop a fully comprehensive coupled atmosphere–fire model of forecast potential in the operational mode. This is not possible at the present time or in the near future. The reasons are that many physical processes in the fire–atmosphere system remain poorly understood and that computational demands of such a modeling approach far exceed the capability of present-day computer technology. The most important use today of physically based fire behavior and transport models is to identify conditions where the current operational empirically based forest fire models are not appropriate. Although unsuitable for faster-than-real-time applications, coupling a fully physically based treatment of the fire combustion and transport with an atmospheric prediction model has the advantage of being able to examine complex wildfire behavior under any set of conditions. Existing fire behavior and fire spread models are faster and easier to use than physically based models and are quite adequate for predicting fire behavior, but only under certain circumstances.

Physically based models will be used to extend existing operational models and to develop new operational models that are suitable for a wider range of conditions.

In the meantime, present capabilities are sufficient to model components of the fire–atmosphere system with a considerable degree of sophistication, as the combustion and atmospheric science research communities show. Given the recent remarkable advances in computer technology, significant development will be made as many model refinements are added.

Finally, we emphasize that convection is the dominant mechanism of fire propagation after the incipient stage of a fire and, despite these objections to the current state of numerical fire modeling, knowledge of the small-scale atmospheric circulations in and around a wildfire is the single most important and elemental improvement that can be made to current wildfire modeling.

APPENDIX I. CIRCULATION AND VORTICITY

Circulation is defined as

$$C \equiv \oint \vec{V} \cdot d\vec{l}$$

where the line integral of fluid velocity $\vec{V}$ is performed over a closed contour, dl is an element length of the contour, and A is the area enclosed by the contour. The line integral is performed in a *counterclockwise* or *positive* direction. Circulation is a scalar quantity and is the macroscopic measure of rotation for a finite area of fluid.

The vorticity vector $\vec{\Omega}$ is defined as

$$\vec{\Omega} = \nabla \times \vec{V}$$

the *curl* of the velocity vector field [&*obar*{V}|ucarrhd|.&] Here $\vec{V} = u\hat{i} + v\hat{j} + w\hat{k}$ is the three-dimensional velocity field and

$$\nabla = \frac{\partial}{\partial x} + \frac{\partial}{\partial y} + \frac{\partial}{\partial z}$$

is the three-dimensional del operator, where $\hat{i}$, $\hat{j}$, and $\hat{k}$ are the unit vectors directed along the x, y, and z Cartesian axes. We are interested in rotation about a horizontal axis or the *vertical* component of vorticity. Therefore we take

$$\hat{k} \cdot \vec{\Omega} = \hat{k} \cdot \nabla \times \vec{V} = \frac{\partial v}{\partial x} - \frac{\partial u}{\partial y}$$

The quantity $\zeta = \hat{k} \cdot \nabla \times \vec{V} = \partial v/\partial x - \partial u/\partial y$ is called *relative* vorticity (i.e., *relative* to the ground).

While circulation is a macroscopic measure of rotation of the fluid, vorticity is a *microscopic* measure of rotation or "spin" of individual particles in a fluid. Relative vorticity is defined as

$$\zeta = \frac{\partial v}{\partial x} - \frac{\partial u}{\partial y} = \lim_{A \to 0} \frac{\oint \vec{V} \cdot d\vec{l}}{A}$$

or the circulation for an infinitesimally small horizontal area A $(A \to 0)$.

To get a physical feeling for vorticity, we use natural coordinates and consider the flow profile in Figure I.1. The natural coordinate system is defined by the orthogonal set of unit vectors $\hat{t}, \hat{n}, \hat{k}$, where $\hat{t}$ is parallel to the horizontal velocity at each point, $\hat{n}$ is normal to the horizontal velocity and directed so that it is positive to the *left* of the flow direction, and $\hat{k}$ is directed vertically upward. $s(x, y, t)$ is the curve followed by a parcel moving in the horizontal plane, and the horizontal velocity is $\vec{V} = V\hat{t}$, where the horizontal speed V is a nonnegative scalar defined by $V \equiv ds/dt$.

The circulation about the circuit in Figure I.1 is

$$C = V[\delta s + d(\delta s)] - \left[V + \frac{\partial V}{\partial n}\delta n\right]\delta s$$

where the negative sign $(-)$ specifies flow direction. Also $\delta n \sin(\delta\beta) \approx \delta n\, \delta\beta = d(\delta s)$ for small angle $\delta\beta$. So

$$C = V\,\delta s + V\,d(\delta s) - V\,\delta s - \frac{\partial V}{\partial n}\delta n\,\delta s$$

$$= V\,\delta n\,\delta\beta - \frac{\partial V}{\partial n}\delta n\,\delta s$$

$$= \left(V\frac{\delta\beta}{\delta s} - \frac{\partial V}{\partial n}\right)\delta n\,\delta s$$

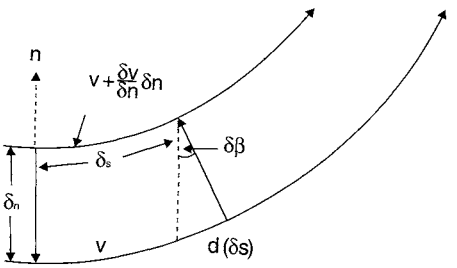

FIGURE I.1 Circulation for an infinitesimal loop in the natural coordinate system.

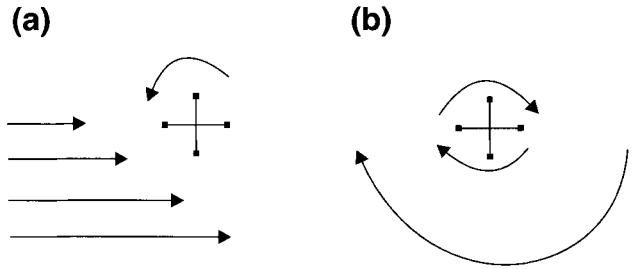

FIGURE I.2 Two types of two-dimensional flow: (a) the rate of change of wind speed normal to the direction of the flow, and (b) the turning of wind following the motion of the air parcel. In (a), a pinwheel in the flow spins cyclonically. In (b), a pinwheel in the flow spins anticyclonically.

But $R\,\delta s = \delta\beta$ where $R \equiv$ radius of curvature following the parcel motion so that

$$C = \left(\frac{V}{R} - \frac{\partial V}{\partial n}\right)\delta n\,\delta s$$

Since the relative vorticity is defined as

$$\zeta = \lim_{A \to 0} \frac{C}{A}$$

we have

$$\zeta = \lim_{\delta n\,\delta s \to 0} \frac{C}{\delta n\,\delta s} = \frac{V}{R} - \frac{\partial V}{\partial n}$$

where V/R is *curvature* vorticity and $\partial V/\partial n$ is *shear* vorticity. Curvature vorticity is the turning of the wind along the parcel motion. Shear vorticity is the rate of change of wind speed normal to the direction of the flow. Figure I.2 illustrates both shear (a) and curvature (b) vorticity. When a small paddle wheel is placed in the flow in Figure I.2a, it turns in the counterclockwise or cyclonic direction. When a small paddle wheel is placed in the flow in Figure I.2b, it turns in the clockwise or anticyclonic direction. Vorticity ζ is *positive* for cyclonic motion and *negative* for anticyclonic motion.

APPENDIX II. DEVELOPMENT OF VERTICAL ROTATION IN A FRICTIONLESS FLUID

The material and concepts discussed in Section II of this chapter are based on the following mathematical representation of vorticity dynamics. In a nonrotat-

ing reference frame (i.e., the Coriolis force due to the Earth's rotation is neglected), conservation of momentum is expressed as

$$\frac{d\vec{V}}{dt} = \frac{\partial \vec{V}}{\partial t} + (\vec{V} \cdot \nabla)\vec{V} = -\frac{1}{\rho}\nabla p - g\hat{k}$$

in a frictionless (or inviscid) fluid. Here $\vec{V} = u\hat{i} + v\hat{j} + w\hat{k}$ is the three-dimensional velocity field and

$$\nabla = \frac{\partial}{\partial x} + \frac{\partial}{\partial y} + \frac{\partial}{\partial z}$$

is the three-dimensional del operator, where $\hat{i}$, $\hat{j}$, and $\hat{k}$ are the unit vectors directed along the Cartesian x, y, and z axes. t is time, ρ is density, p is pressure, and g is the acceleration due to gravity. The force due to friction is neglected. The vector identity

$$(\vec{V} \cdot \nabla)\vec{V} = \nabla\left(\frac{\vec{V} \cdot \vec{V}}{2}\right) - \vec{V} \times \nabla \times \vec{V}$$

is used to rewrite the conservation of momentum equation as

$$\frac{\partial \vec{V}}{\partial t} = -\nabla\left(\frac{\vec{V} \cdot \vec{V}}{2}\right) + \vec{V} \times \vec{\Omega} - \frac{\nabla p}{\rho} - g\hat{k} \qquad \text{(II.A)}$$

where $\vec{\Omega} = \nabla \times \vec{V}$. Taking the curl ($\nabla \times$) of Eq. (II.A), and recalling that the curl of the gradient vanishes, gives

$$\frac{\partial \vec{\Omega}}{\partial t} = \nabla \times (\vec{V} \times \vec{\Omega}) - \nabla \times \frac{\nabla p}{\rho} \qquad \text{(II.B)}$$

Let $\zeta = \hat{k} \times \vec{\Omega} = \hat{k} \cdot \nabla \times \vec{V}$, the vertical component of the vorticity (Appendix I). Taking $\hat{k} \cdot$ of Eq. (II.B) gives

$$\frac{\partial \zeta}{\partial t} = \hat{k} \cdot \nabla \times (\vec{V} \times \vec{\Omega}) - \hat{k} \cdot \nabla\left(\frac{1}{\rho}\right) \times \nabla p \qquad \text{(II.C)}$$

the vertical vorticity equation. After some algebraic manipulation, it is possible to rewrite Eq. (II.C) as

$$\begin{aligned} \frac{\partial \zeta}{\partial t} = {} & -\vec{V}_h \cdot \nabla_h \zeta - w\frac{\partial \zeta}{\partial z} - \zeta \nabla_h \cdot \vec{V}_h \\ & + \hat{k} \cdot \left(\frac{\partial \vec{V}_h}{\partial z} \times \nabla_h w\right) + \frac{1}{\rho^2}\left(\frac{\partial \rho}{\partial x}\frac{\partial p}{\partial y} - \frac{\partial \rho}{\partial y}\frac{\partial p}{\partial x}\right) \end{aligned} \qquad \text{(II.D)}$$

where $\vec{V}_h = u\hat{i} + v\hat{k}$ is the two-dimensional horizontal wind and ∇_h is the horizontal gradient in the x-y plane. Each term in Eq. (II.D) has a physical interpretation.

Term $\partial\zeta/\partial t$ is the *local* time change of vertical vorticity. Rather than attach our coordinate system to moving fluid parcels, we determine the rate of change of ζ for the fluid at a fixed point or location on the Earth's surface. Each term on the right-hand side of Eq. (II.D) contributes to the local rate of change of ζ.

Term $-\vec{V}_h \cdot \nabla_h\zeta$ is the advection of vorticity by the horizontal wind. For example, wind blowing from a region of positive vorticity toward a region of negative vorticity contributes positively to the local vorticity change. Term $-w(\partial\zeta/\partial z)$ is the advection of vorticity by the vertical wind, and its effect is similar to horizontal advection of vorticity except that it redistributes vorticity ζ in the vertical direction.

Term $-\zeta\nabla_h \cdot \vec{V}_h$ represents changing vorticity due to horizontal divergence. It is the fluid analog of the change in angular velocity resulting from a change in the moment of inertia of a solid body when angular momentum is conserved. If there is positive horizontal divergence, the area enclosed by a chain of fluid parcels increases with time, and if the circulation is to be conserved, the average vorticity of the enclosed fluid must decrease. This term is called the divergence or stretching term. If it is assumed that the three-dimensional flow is nondivergent, $\nabla \cdot \vec{V} = 0$, then

$$-\frac{\partial w}{\partial z} = \frac{\partial u}{\partial x} + \frac{\partial v}{\partial z}$$

Substituting this into the divergence term gives

$$-\zeta\nabla_h \cdot \vec{V}_h = \zeta\frac{\partial w}{\partial z}$$

Vertical motion is responsible for the "stretching" effect. When vertical motion narrows the diameter of the area enclosed by the chain of fluid parcels (horizontal convergence), vorticity increases.

Term $\hat{k} \cdot (\partial\vec{V}_h/\partial z \times \nabla_h w)$ represents the generation of vertical vorticity by the tilting of horizontally oriented components of vorticity into the vertical by a nonuniform vertical motion field. This term is called the twisting or tilting term and is illustrated in Figure 1 and described in Section II.

Term $-\hat{k} \cdot \nabla(1/p) \times \nabla p = (1/\rho^2)[(\partial\rho/\partial x)(\partial p/\partial y) - (\partial\rho/\partial y)(\partial p/\partial x)]$ is called the *solenoidal* term. It is illustrated in Figure 2 and described in Section II. To illustrate possible production of vertical vorticity by the solenoidal term, consider what happens to a small rectangular parcel or bar of fluid in the situation depicted in Figure 2. Imagine a pressure gradient in the fluid, perpendicular to the parcel and uniform along its length; in this case, the parcel moves through

the fluid from high to low pressure. Now imagine that the fluid density is not constant, but is larger at one end of the parcel than the other. The forces $\vec{F}_{y_1}$ and $\vec{F}_{y_2}$ can be written

$$\vec{F}_{y_1} = -\frac{1}{\rho_1}\frac{\partial p}{\partial y}\hat{j}, \qquad \vec{F}_{y_2} = -\frac{1}{\rho_2}\frac{\partial p}{\partial y}\hat{j}$$

Since

$$\rho_1 > \rho_2, \qquad \frac{1}{\rho_1} < \frac{1}{\rho_2}$$

then

$$|\vec{F}_{y_1}| < |\vec{F}_{y_2}|$$

and the torque applied by the pressure gradient forces, $\vec{F}_{y_1}$ and $\vec{F}_{y_2}$, causes the fluid bar to rotate counterclockwise. Thus when the gradient of pressure ∇p and the gradient of density $\nabla \rho$ are not parallel, the parcel experiences a torque that causes it to rotate, producing vorticity.

The advection terms distribute existing ζ, while the stretching or divergence term "spins up" or "spins down" existing vorticity. Only the tilting and solenoidal terms *generate* vertical vorticity ζ in Eq. (II.D) in an inviscid fluid. And although friction in the fluid is not included in this discussion, *turbulent* or *frictional drag* can be both a source and sink of local rotation.

A. Vertically Rotating Convective Cells in a Mean Wind Field

Imagine a flow field as in Figure II.1 consisting of a single convective updraft embedded in a background flow $\overline{U}$ which is a function of height z only and westerly in the positive $\hat{i}$ direction. Let

$$\vec{\Omega} = \frac{d\overline{U}}{dz}\hat{j} + \vec{\Omega}'(x, y, z, t), \qquad \vec{V} = \overline{U}(z)\hat{i} + \vec{V}'(x, y, z, t),$$

$$p = \overline{p}(z) + p'(x, y, z, t), \qquad \text{and} \qquad \rho = \overline{\rho}(z)$$

where it is assumed for simplicity that density does not vary in the horizontal and is a function of height only. The overbar ($\overline{\ }$) denotes the background or base state, and the prime ($'$) denotes fluctuations due to convection or perturbations from the background or base state. Substituting $\vec{\Omega}$, $\vec{V}$, ρ, and p into the right-hand side of Eq. (II.D) gives

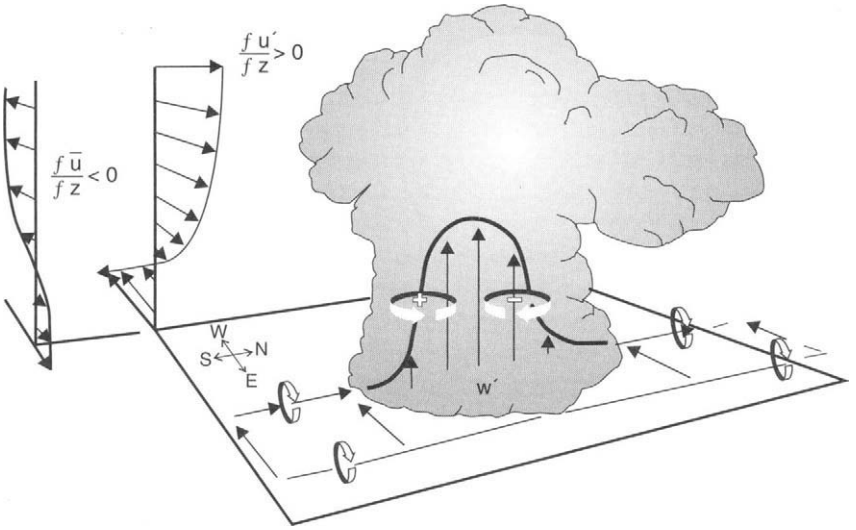

FIGURE II.1 Development of rotation in a single convective updraft (shown by arrows) along a fire front embedded in a background with mean wind $\bar{u}$ decreasing with height (shown by wind arrows in the upper left corner). Heavy solid lines show vortex lines with sense of rotation shown by circulation arrows. Plus and minus signs indicate cyclonic and anticyclonic rotation caused by vortex tube tilting.

$$\frac{\partial \zeta'}{\partial t} = -\vec{V}_h' \cdot \nabla_h \zeta' - \overline{U}\frac{\partial \zeta'}{\partial x} - w'\frac{\partial \zeta'}{\partial z} - \zeta' \nabla_h \cdot \vec{V}_h' + \frac{\partial w'}{\partial y}\frac{\partial \overline{U}}{\partial z} + \hat{k} \cdot \left(\frac{\partial \vec{V}_h'}{\partial z} \times \nabla_h w' \right) \tag{II.E}$$

For this flow field, there is no generation of vertical vorticity by the solenoidal effect, and in Eq. (II.E) vertical vorticity is produced only by tilting the horizontal vorticity into the vertical:

$$\frac{\partial w'}{\partial y}\frac{\partial \overline{U}}{\partial z} + \hat{k} \cdot \left(\frac{\partial \vec{V}_h'}{\partial z} \times \nabla_h w' \right) = \frac{\partial w'}{\partial y}\frac{\partial \overline{U}}{\partial z} + \frac{\partial w'}{\partial y}\frac{\partial u'}{\partial z} - \frac{\partial w'}{\partial x}\frac{\partial v'}{\partial z}$$

The terms on the right-hand side of this expression are, respectively, the tilting by the perturbed differential vertical motion field $(\partial w'/\partial y, \partial w'/\partial x)$ of linear horizontal vorticity $(\partial \overline{U}/\partial z)$ and perturbed horizontal vorticity $(\partial u'/\partial z, \partial v'/\partial z)$.

For forced convection, such as in a wildfire, the perturbation portion of the dependent variables can be as large or larger than the mean or basic state portion. When perturbation variables and products of perturbation variables dominate, the effect by the tilting of horizontal vorticity of the base state, $\partial \overline{U}/\partial z$, is

negligible compared to the tilting of horizontal shear in the convective flow, $\partial u'/\partial z$ and $\partial v'/\partial z$.

Say fire convection produces vertical wind shears where $\partial u'/\partial z > 0$. This happens for east winds ($u' < 0$) stronger at the surface, decreasing with height, or west winds ($u' > 0$) weaker at the surface, increasing with height. This positive vertical wind shear of u' coupled with $\partial w'/\partial y > 0$ south of the updraft core and $\partial w'/\partial y < 0$ north of the updraft core produces—once tilting of horizontal vorticity has occurred—two centers of vertical vorticity. The one south of the updraft core has counterclockwise or positive rotation; the one north has clockwise or negative rotation. This is similar, but opposite to, the situation depicted in Figure 1(c) (Section II). If the perturbation product $(\partial w'/\partial y)(\partial u'/\partial z)$ is the dominate tilting term in Eq. (II.E), then $\partial \zeta'/\partial t$ is increased south and decreased north of the updraft core.

Once ζ' exists, both advection of the perturbed vorticity by the basic state flow, $-\overline{U}(\partial \zeta'/\partial x)$, and by the perturbed horizontal wind, $-\vec{V}_h' \cdot \nabla_h \zeta'$, can contribute to the local time change of perturbation vorticity owing to the air motion. If a background wind $\overline{U}$ blows from a region of positive perturbation vorticity ($\zeta' > 0$) toward a region negative or no perturbation vorticity ($\zeta' \leq 0$), the advection of perturbed vorticity by the basic state flow contributes positively to the local perturbation change, and $\partial \zeta'/\partial t$ in Eq. (II.E) is increased. For the situation depicted in Figure II.1, the mean wind $\overline{u}$ will advect fire-generated vorticity ζ' east of the fire at low levels, and west of the fire at upper levels.

And once ζ' exists, the stretching term $-\zeta' \nabla_h \cdot \vec{V}_h'$ can either increase or decrease ζ' locally for horizontal winds converging or diverging, respectively, while the vertical advection term $-w'(\partial \zeta'/\partial z)$ can redistribute vorticity in the vertical. For example, upper-level vorticity can be advected to the surface by convective downdrafts.

Density does vary in all three directions, and the solenoidal effect in Eqs. (II.D) and (II.E) generates perturbed vertical vorticity that also is advected by the background wind and convectively perturbed flow and is increased or decreased by horizontal convergence and stretching. And finally, the fluid is not frictionless. Although friction and turbulence can increase local rotation, they are also crucial for the destruction of local rotation.

APPENDIX III. GENERATION OF VERTICAL MOTION IN ROTATING CONVECTIVE CELLS

Even rotating convective cells with relatively low buoyancy can produce low-level updrafts that are as strong or even stronger than their high-buoyancy counterparts. The reason for this is that the strength of vertical motion in rotating convective cells is not only dependent on buoyancy forcing. Acceleration

in the core of a rotating convective cell is principally governed by buoyancy and the vertical gradient of perturbation pressure.

The total buoyancy of an air parcel is due to thermal (sensible, latent, and radiational) heating and the effect of condensate loading, while vertically directed pressure gradient forces are attributed to the so-called "centrifugal pump" effect. Section II and Appendix II describe how cyclonic and anticyclonic vertically rotating vortices can develop in a fire. As soon as a vertical vortex is established, vertical motion in the center of the vortex develops. To understand the generation of the vertical motion, take the $\nabla\cdot$ of Eq. (II.A) to yield

$$\nabla^2\left(\frac{p}{\rho}\right) = -\nabla^2\frac{(\vec{V}\cdot\vec{V})}{2} + \nabla\cdot(\vec{V}\times\vec{\Omega}) \qquad \text{(III.A)}$$

where $\nabla\cdot\vec{V} = 0$ is assumed. Terms $-\nabla^2[(\vec{V}\cdot\vec{V})/2]$ and $\nabla(\vec{V}\times\vec{\Omega})$ represent dynamical forcing, and we are interested in the effect of dynamical forcing on the pressure field in a vertical vortex. We use cylindrical coordinates (r, λ, z) centered on the axis of rotation (Figure III.1) to investigate the pressure variation in a vortex. Here λ is azimuthal angle, $\hat{j}_\lambda$ is the unit vector in the azimuthal direction (with positive counterclockwise), z is vertical height, r is the radial distance from the axis of rotation, and $\hat{i}_\lambda$ is the unit vector in the r direction.

For pure rotation about a vertical z axis, the horizontal velocity field and vertical component of vorticity in cylindrical coordinates are, respectively,

$$\vec{V} = v_\lambda\hat{j} \qquad \text{and} \qquad \hat{k}\cdot\vec{\Omega} = \zeta = \frac{1}{r}\frac{\partial}{\partial r}(rv_\lambda)$$

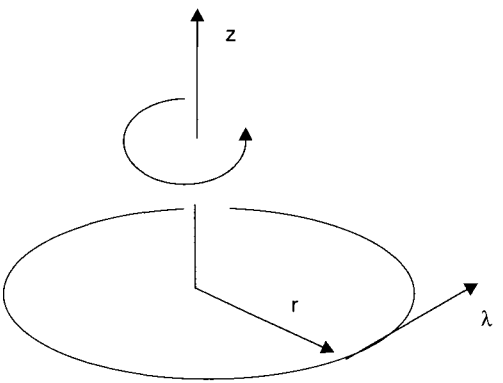

FIGURE III.1 The cylindrical coordinate system.

Therefore,

$$\hat{V} \times \vec{\Omega} = \frac{v_\lambda}{r} \frac{\partial}{\partial r}(r_\lambda v_\lambda)\hat{i}_\lambda$$

Assuming that the vertical scale is much larger than the radial scale, the Laplacian ∇^2 in cylindrical coordinates is approximately

$$\nabla^2 \approx \frac{1}{r} \frac{\partial}{\partial r}\left(r \frac{\partial}{\partial r}\right)$$

Substituting into Eq. (III.A), the dynamical component of the pressure perturbation in the vortex is expressed as

$$\begin{aligned} \frac{1}{r} \frac{\partial}{\partial r}\left(\frac{r}{\rho_0} \frac{\partial p_{dyn}}{\partial r}\right) &\approx -\frac{1}{r} \frac{\partial}{\partial r}\left[r \frac{\partial(v_\lambda^2/2)}{\partial r}\right] + \frac{1}{r} \frac{\partial}{\partial r}\left[v_\lambda \frac{\partial}{\partial r}(r v_\lambda)\right] \\ &\approx \frac{1}{r} \frac{\partial v_\lambda^2}{\partial r} \end{aligned} \tag{III.B}$$

where $\rho = \rho_0$ and is considered constant in the radial direction. Integrating Eq. (III.B) with respect to r gives

$$\frac{1}{\rho_0} \frac{\partial p_{dyn}}{\partial r} \approx \frac{v_\lambda^2}{r}$$

an equation for cyclostrophic balance, where the pressure gradient force $(1/\rho_0)(\partial p_{dyn}/\partial r)$ is always directed *inward*, toward the center of rotation, while the centrifugal force v_λ^2/r is always directed *outward*. The *low* pressure at the center of (either clockwise or counterclockwise) rotation provides a pressure gradient force to balance the outward centrifugal force.

This *dynamically* generated low pressure at in the center of the vortex produces a *vertically* directed pressure gradient force. Since air is accelerated from high to low pressure, the result is the development of an updraft from below, or a downdraft from above, in the rotating core. This is the centrifugal pump effect.

NOTATION

Roman Letters

c_p	specific heat capacity of dry air at constant p	J kg^{-1} K^{-1}
g	magnitude of acceleration due to gravity	m s^{-2}

p	pressure	Pa
s	distance along a parcel trajectory	m
t	time	s
u, v, w	wind components in x (eastward), y (northward), and z (vertical) directions	$m\ s^{-1}$
v_f	rate of spread at the head of a wind-aided fire	$m\ s^{-1}$
x, y, z	distances in the east–west, north–south, and vertical directions; Cartesian coordinates parallel to, and perpendicular to, the ground	m
C	fluid circulation	$m^2\ s^{-1}$
$\vec{F}$	a force	$kg\ m\ s^{-2}$
F_s	sensible heat flux	$W\ m^{-2}$
F_{r_c}	convective Froude number	
T	absolute temperature	K
T_{IR}	infrared T measurement	K
U	ambient air wind speed	$m\ s^{-1}$
U_0	relative speed of air passing over the fire	$m\ s^{-1}$
V	speed in natural coordinates	$m\ s^{-1}$
$\vec{V}$	fluid velocity	$m\ s^{-1}$
W_f	width of region of intense heating	m
τ	burn time of small fuel	s
Δt	time step	s
Δw	w anomaly over region of intense heating;	$m\ s^{-1}$
	change in w over Δz	$m\ s^{-1}$
Δx_{fuel}	fuel grid cell size in horizontal direction	m
$\Delta x, \Delta y, \Delta z$	distances or grid cell sizes in x, y, and z directions	m
ΔT	T anomaly over region of intense heating	K
ζ	vertical component of relative vorticity	s^{-1}
ρ	air density	$kg\ m^{-3}$
$\vec{\Omega}$	vorticity vector	s^{-1}
∇	three dimensional gradient or del operator	m^{-1}
$\hat{i}, \hat{j}, \hat{k}$	unit vectors along x, y, and z axes	

CYLINDRICAL COORDINATES

$\hat{t}, \hat{n}$	unit vectors normal and parallel to fluid parcel trajectory
β	angular direction of the wind or fluid flow
R	radius of curvature following the parcel motion
λ, r	asimuthal angle, radial distance from axis
$\hat{j}_\lambda, \hat{i}_\lambda$	unit vectors in the asimuthal and r directions
u_λ	velocity component in the asimuthal direction

SPECIAL NOTATION

--	a background or base state; time and area average
< >	horizontal average or mean value
′	fluctuations or perturbations from a background or base state; fluctuations or perturbations from the horizontal average
^	unit vector

REFERENCES

Baines, P. (1990). Physical mechanisms for the propagation of surface fires. *Math. Comput. Modeling,* **13**, 83–94.

Banta, R. M., Olivier, L. D., Holloway, E. T., Kropfli, R. A., Bartram, B. W., Cupp, R. E., and Post, M. J. (1992). Smoke column observations from two forest fires using Doppler lidar and Doppler radar. *J. Appl. Meteorol.* **31**, 1328–1349.

Bossert, J. E., Linn, R. R., Reisner, J. M., Winterkamp, J. L., Dennison, P., and Roberts, D. (2000). Coupled atmosphere–fire behavior model sensitivity to spatial fuels characterization. Preprints of "3rd Symp. Fire and Forest Meteorology," Amer. Meteor. Soc. 80th Annual Meeting, Los Angeles, CA, pp. 21–26.

Byram, G. M. (1973). Combustion of forest fuels. "Forest Fire, Control and Use" (A. A. Brown and K. P. Davis, Eds. 2nd ed., pp. 155–182. McGraw-Hill, New York.

Chandler, C., Cheney, P., Thomas, P., Trabaud, L., and Williams, D. (1983). "Fire in Forestry Forest Fire Behavior and Effects." John Wiley and Sons, New York.

Church, C. R., and Snow, J. T. (1979). The dynamics of natural tornadoes as inferred from laboratory simulations. *J. Rech. Atmos.* **12**, 111–133.

Church, C. R., Snow, J. T., and Dessens, J. (1980). Intense atmospheric vortices associated with a 100 MW fire. *Bull. Amer. Meteor. Soc.* **61**, 682–694.

Clark, T. L., Radke, L., Coen, J. L., and Middleton, D. (1999). Analysis of small-scale convective dynamics in a crown fire using infrared video camera imagery. *J. Appl. Meteorol.* **38**, 1401–1420.

Clark, T. L., Jenkins, M. A., Coen, J., and Packham, D. R. (1996a). A coupled atmospheric–fire model: Role of the convective Froude number and dynamic fingering at the fire line. *Int. J. Wildland Fire* **6**(4), 177–190.

Clark, T. L., Jenkins, M. A., Coen, J., and Packham, D. R. (1996b). A coupled atmospheric–fire model: Convective feedback on fire line dynamics. *J. Appl. Meteorol.* **35**, 875–901.

Coen, J. L., Clark, T. L., and Hall, W. D. (1998). Simulations of the effect of terrain on fire behavior: Experiments using a coupled atmosphere–fire model. Preprints of "2nd Symp. Fire and Forest Meteorology," Amer. Meteor. Soc., Phoenix, AZ, pp. 87–90.

Corlett, R. C. (1974). Fire violence and modeling (Chapter 6). *In* "Heat Transfer in Fires: Thermophysics, Social Impacts, Economic Impact." Scripta Book Company, Hemisphere Publishing Corporation, Washington, DC.

Gall, R. L. (1982). Internal dynamics of tornado-like vortices. *J. Atmos. Sci.* **39**, 2721–2736.

Heilman, W. E. (1992). Atmospheric simulations of extreme surface heating episodes on simple hills. *Int. J. Wildland Fire* **2**, 99–114.

Heilman, W. E., and Fast, J. D. (1992). Simulations of horizontal roll vortex development above lines of extreme surface heating. *Int. J. Wildland Fire* **2**, 55–68.

Kim, J., and Moin, P. (1986). The structure of the vorticity field in turbulent channel flow. Part 2. Study of ensemble-averaged fields. *J. Fluid Mech.* **162**, 339–363.

King, A. R. (1964). Characteristics of a fire-induced tornado. *Australian Meteorological Magazine* No. 44, pp. 1–9.

Linn, R. R. (1997). "A Transport Model for Prediction of Wildfire Behavior." Los Alamos National Laboratory thesis LA-13334-T, New Mexico State University.

Linn, R. R., and Harlow, F. H. (1998). FIRETEC: A transport description of wildfire behavior. Preprints of "2nd Symp. Fire and Forest Meteorology," Amer. Meteor. Soc. 78th Annual Meeting, Phoenix, AZ, pp. 14–19.

Linn, R. R., Bossert, J. E., Harlow, F., Reisner, J. M., and Smith, S. (2000). Studying complex wildfire behavior using FIRETEC. Preprints of "3rd Symp. Fire and Forest Meteorology," Amer. Meteor. Soc. 80th Annual Meeting, Los Angeles, CA, pp. 15–20.

McGrattan, K., Baum, H. R., and Rehm, R. G. (1996). Numerical simulation of smoke plumes from large oil fires. *Atmos. Environ.* **30**(24), 4125–4136.

McRae, D. J., and Stocks, B. J. (1987). Large-scale convection burning in Ontario. "Proc. 9th Conf. on Fire and Forest Meteorology," San Diego, pp. 23–29.

McRae, D. J., Stocks, B. J., and Ogilvie, C. J. (1989). Fire acceleration on large-scale convection burns. "Proc. 10th Conf. on Fire and Forest Meteorology," Ottawa, pp. 101–107.

McRae, D. J., and Flannigan, M. D. (1990). Development of large vortices on prescribed fires. *Can. J. For. Res.* **20**, 1878–1887.

Moin, P., and Kim, J. (1982). Numerical investigation of turbulent channel flow. *J. Fluid Mech.* **118**, 341–377.

Radke, L. F., Clark, T. L., Coen, J. L., Walther, C., Lockwood, R., Riggan, P. J., Brass, J., and Higgins, R. (2000). The WildFire Experiment: Observations with Airborne Remote Sensors. *Can. J. Remote Sensing* **26**(5), 406–417.

Reisner, J. M., Bossert, J. E., and Winterkamp, J. L. (1998). Numerical simulations of two wildfire events using a combined modeling system (HI-GRAD/BEHAVE). Preprints of "2nd Symp. Forest and Fire Meteorology," Amer. Meteor. Soc. 78th Annual Meeting, Phoenix, AZ, pp. 6–13.

Reisner, J. M., Swynne, S., Margolin, L., and Linn, R. R. (2000). Coupled-atmosphere fire modeling using the method of averaging. *Mon. Wea. Review,* **128**, 3683–3691.

Rothermel, R. C. (1972). "A Mathematical Model for Predicting Fire Spread in Wildland Fuels." Research Paper INT-115. USDA Forest Service, Intermountain Forest and Range Experiment Station, Ogden, UT.

Strauss, D., Bednar, L., and Mees, R. (1989). Do one percent of forest fires cause ninety-nine percent of the damage? *For. Sci.* **35**(2), 319–328.

Weiss, D. R., and Biging, G. S. (1996). Effects of wind velocity and slope on flame properties. *Can. J. For. Res.* **26**, 1849–1858.

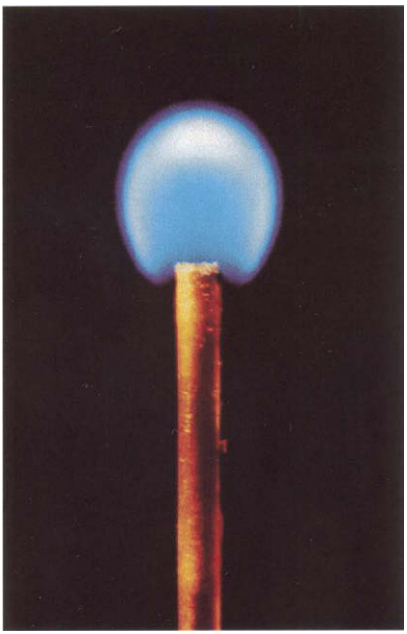

CHAPTER 2, FIGURE 3 An ethylene-air microdiffusion flame established on a 0.25-mm-diameter hypodermic needle (fuel flow rate at the burner port is 2 m/s). From Ban *et al.* (1994). *J. Heat Transfer* **116**, 331.

CHAPTER 2, FIGURE 4 A hydrogen-air jet diffusion flame established on a 1.43-mm-diameter stainless-steel burner nozzle (hydrogen flow rate at the burner port is 500 m/s) (Takahashi *et al.*, 1996).

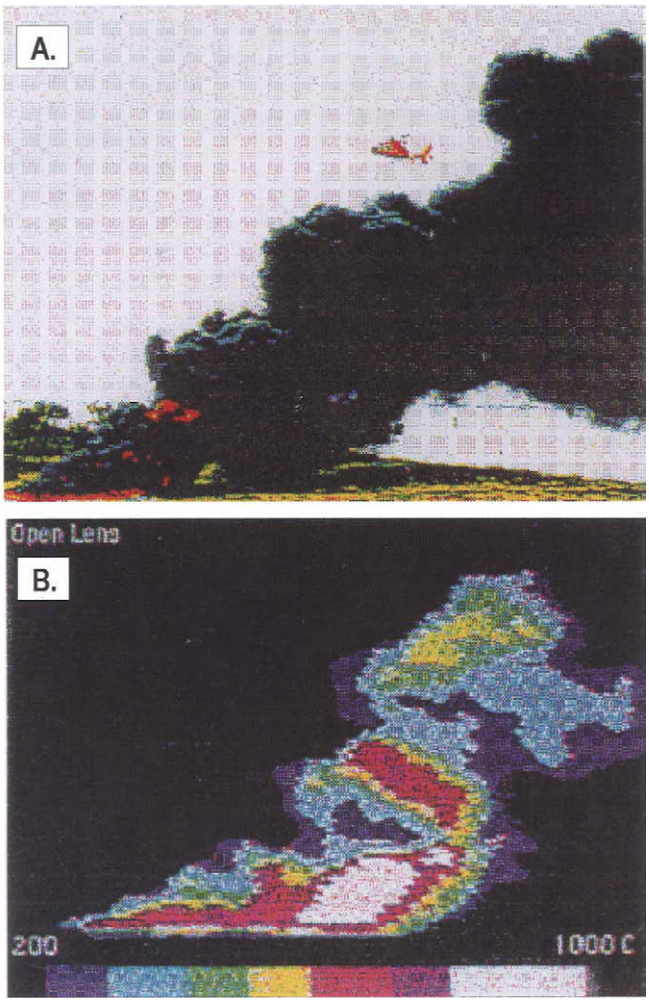

CHAPTER 2, FIGURE 9 (A) A diesel oil pool fire using a 15-m square shape open-top container (the test was conducted by the Building and Fire Research Laboratory at the National Institute of Standards and Technology, at the U.S. Coast Guard Fire and Safety Test Detachment in Mobile, AL). (B) An infrared image of the flame in Figure 9A.

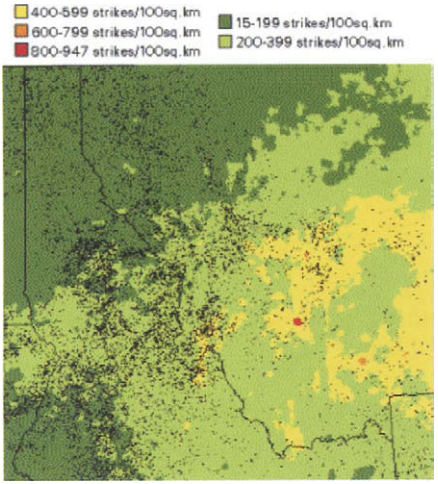

CHAPTER 11, FIGURE 1 Fire locations (black points) with lightning density (flashes/100 km^2) as background.

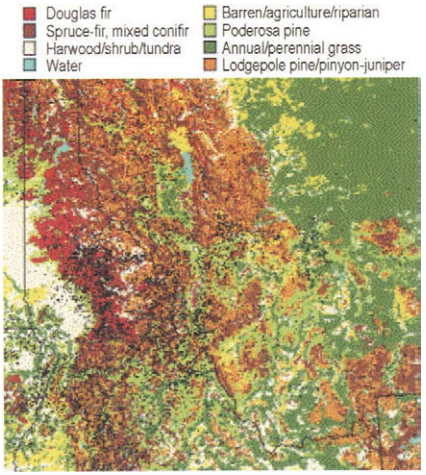

CHAPTER 11, FIGURE 2 Fire locations (black points) with fuel type as background.

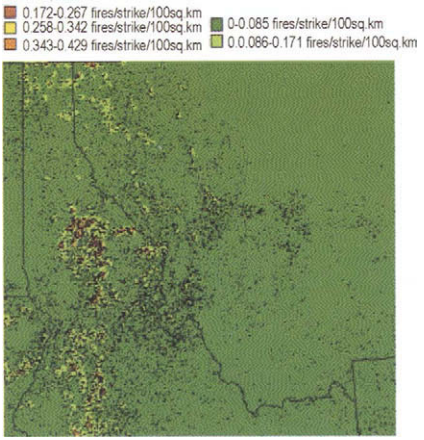

CHAPTER 11, FIGURE 3 Fire locations (black points) with ignition efficiency as background.

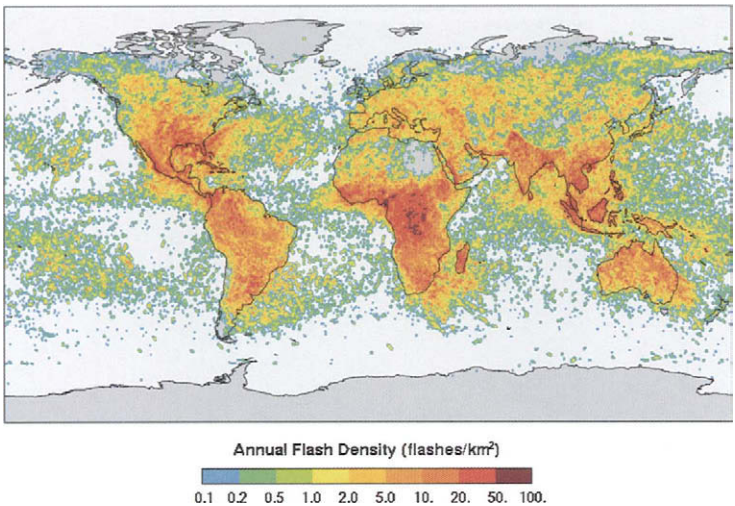

CHAPTER 11, FIGURE 18 Worldwide lightning map as observed by the Optical Transient Detector in 1997. Courtesy of Global Hydrology and Climate Center and NASA/MSFC.

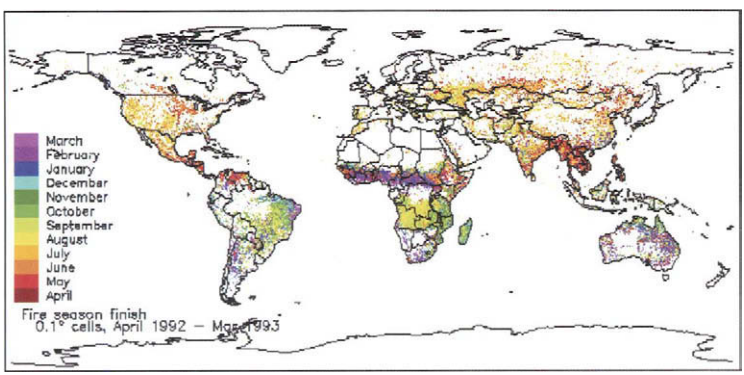

CHAPTER 11, FIGURE 19 World Fires, April 1992–May 1993 (courtesy of Dwyer *et al.*, 1999).